Reduced Rainfall in Future Heavy Precipitation Events Related to Contracted Rain Area Despite Increased Rain Rate

Moshe Armon[1,1], Francesco Marra[2,2], Yehouda Enzel[1,1], Dorita Rostkier-Edelstein[3,3], Chaim I Garfinkel[1,1], Ori Adam[4,4], Uri Dayan[5,5], and Efrat Morin[6,6]

[1]Hebrew University of Jerusalem
[2]Institute of Atmospheric Sciences and Climate, National Research Council
[3]Department of Environmental Physics, Environmental Sciences Division, IIBR
[4]Hebrew University
[5]Department of Geography, Hebrew University of Jerusalem
[6]Institute of Earth Sciences, The Hebrew University of Jerusalem

November 30, 2022

Abstract

Heavy precipitation events (HPEs) can lead to deadly and costly natural disasters and are critical to the hydrological budget in regions where rainfall variability is high and water resources depend on individual storms. Thus, reliable projections of such events in the future are needed. To provide high-resolution projections under the RCP8.5 scenario for HPEs at the end of the 21st century and to understand the changes in sub-hourly to daily rainfall patterns, weather research and forecasting (WRF) model simulations of 41 historic HPEs in the eastern Mediterranean are compared with "pseudo global warming" simulations of the same events. This paper presents the changes in rainfall patterns in future storms, decomposed into storms' mean conditional rain rate, duration, and area. A major decrease in rainfall accumulation (-30% averaged across events) is found throughout future HPEs. This decrease results from a substantial reduction of the rain area of storms (-40%) and occurs despite an increase in the mean conditional rain intensity (+15%). The duration of the HPEs decreases (-9%) in future simulations. Regionally maximal 10-min rain rates increase (+22%), whereas over most of the region, long-duration rain rates decrease. The consistency of results across events, driven by varying synoptic conditions, suggests that these changes have low sensitivity to the specific large-scale flow during the events. Future HPEs in the eastern Mediterranean will therefore likely be drier and more spatiotemporally concentrated, with substantial implications on hydrological outcomes of storms.

Reduced Rainfall in Future Heavy Precipitation Events Related to Contracted Rain Area Despite Increased Rain Rate

Moshe Armon[1], Francesco Marra[2], Yehouda Enzel[1], Dorita Rostkier-Edelstein[1,3], Chaim I. Garfinkel[1], Ori Adam[1], Uri Dayan[4], Efrat Morin[1]

[1]Fredy and Nadine Herrmann Institute of Earth Sciences, the Hebrew University of Jerusalem, Jerusalem, 9190401, Israel

[2]National Research Council of Italy, Institute of Atmospheric Sciences and Climate, CNR-ISAC, Bologna 40129, Italy.

[3]Department of Environmental Physics, Environmental Sciences Division, IIBR, Ness-Ziona 7410001, Israel.

[4]Department of Geography, the Hebrew University of Jerusalem, Jerusalem, 9190401, Israel.

Corresponding author: Moshe Armon (moshe.armon@mail.huji.ac.il)

Key Points:

- End of 21st century heavy precipitation events in the eastern Mediterranean are projected to have substantially reduced rainfall yield
- This reduction results mainly from a major decrease in rain area during future events, despite the increased conditional rain rate
- Changes in rain yield, rate, and area are consistent across many events, suggesting great hydrological implications for the region

Abstract

Heavy precipitation events (HPEs) can lead to deadly and costly natural disasters and are critical to the hydrological budget in regions where rainfall variability is high and water resources depend on individual storms. Thus, reliable projections of such events in the future are needed. To provide high-resolution projections under the RCP8.5 scenario for HPEs at the end of the 21st century and to understand the changes in sub-hourly to daily rainfall patterns, weather research and forecasting (WRF) model simulations of 41 historic HPEs in the eastern Mediterranean are compared with "pseudo global warming" simulations of the same events. This paper presents the changes in rainfall patterns in future storms, decomposed into storms' mean conditional rain rate, duration, and area. A major decrease in rainfall accumulation (-30% averaged across events) is found throughout future HPEs. This decrease results from a substantial reduction of the rain area of storms (-40%) and occurs despite an increase in the mean conditional rain intensity (+15%). The duration of the HPEs decreases (-9%) in future simulations. Regionally maximal 10-min rain rates increase (+22%), whereas over most of the region, long-duration rain rates decrease. The consistency of results across events, driven by varying synoptic conditions, suggests that these changes have low sensitivity to the specific large-scale flow during the events. Future HPEs in the eastern Mediterranean will therefore likely be drier and more spatiotemporally concentrated, with substantial implications on hydrological outcomes of storms.

Plain Language Summary

Heavy precipitation events are large storms that can recharge freshwater reservoirs, but can also lead to hazardous outcomes such as flash floods. Therefore, understanding the impacts of climate change on such storms is critical. Here, a weather model similar to those used in weather forecasts is used to simulate heavy precipitation events in the eastern Mediterranean. A large collection of storms is simulated in pairs: (1) historic storms, known for their high impact, and (2) placing the same storms in a global warming scenario projected for the end of the 21st century. Using these simulations we ask how present-day storms would look like were they to occur at the warmer end of the 21st century. The future storms are found to produce much less rainfall compared to the historic ones. This decrease in rainfall is attributed mainly to the reduction in the area covered by storms' rainfall, and happens despite increasing rainfall intensities. These results suggest that the region will be drier in the future with larger dry areas during storms; however, over short durations, it would rain more intensely over contracted areas – increasing local hazards associated with heavy precipitation events.

1 Introduction

Expected impacts of climate change on rainfall during heavy precipitation events (HPEs) have the potential to significantly alter their influence on future societies. Where precipitation variability is high, such as in Mediterranean and arid climates, the impact of individual HPEs in terms of both peril (e.g., Borga et al., 2014; Dayan et al., 2021; Raveh-Rubin & Wernli, 2016; Rinat et al., 2020; De Vries et al., 2013) and water resources (Flaounas et al., 2021; Nasta et al., 2018; Samuels et al., 2009; R. G. Taylor et al., 2013) is great, and reliable projections of HPEs are needed (e.g., Sillmann et al., 2021).

Individual HPEs are controlled by specific large scale and synoptic circulation patterns. However, projected changes in the atmospheric circulation are highly uncertain across global climate models (GCMs) due to the wide variety of factors at play (Shepherd, 2014).

Furthermore, climate change impact on HPEs can be quite different from the well-studied impact on the mean rainfall or even on high precipitation percentiles (e.g., Donat et al., 2016; Kendon et al., 2018; Moustakis et al., 2021; O'Gorman, 2015; Pfahl et al., 2017; Trenberth et al., 2015).

Detailed projections of the regional rainfall during a specific event can only be provided by models that can explicitly resolve the convective processes governing precipitation during HPEs (e.g., Fosser et al., 2014). Indeed, convection-permitting models (CPMs) are more reliable than GCMs in simulating spatiotemporal precipitation patterns (Ban et al., 2014; Cannon & Innocenti, 2019; Crook et al., 2019; Kendon et al., 2014; Meredith et al., 2020; Poujol et al., 2020; Prein et al., 2015, 2017; Westra et al., 2014). Recent methodological and computing advances enable "climate" CPM simulations with long-term (~10 yr), large-scale (continental), and high resolution (a few kilometers) outputs with some groups already running ensemble simulations over specific regions (Chan et al., 2020; Coppola et al., 2020; Pichelli et al., 2021). These give probabilistic projections of changes in precipitation extremes with expectations to achieve better quantification of future HPEs (e.g., Kendon et al., 2014; Poujol et al., 2020). However, rare extreme or heavy precipitation events are, by definition, hard to assess even with such simulations (e.g., Fatichi et al., 2016; Kendon et al., 2021). Moreover, a few kilometers resolution may still not be sufficient to represent the local nature of convective clouds, especially when shallow convection is present (Kendon et al., 2021; Prein et al., 2015). Therefore, trying to provide reliable projections of the changes in rainfall patterns during HPEs will probably take many more years of improvement in climate modeling. A complementing approach, aimed at resolving extreme events and intra-event characteristics (Fowler, Ali, et al., 2021; O'Gorman, 2015), is to provide projections of specific high impact events either by identifying interesting events such as hurricanes over long-term simulations (Gutmann et al., 2018), or through the simulation of individual events known for their high-impact, such as snowstorms (G. Chen et al., 2020), tropical cyclones (J. Chen et al., 2020), or HPEs (Ferreira, 2021).

Pseudo global warming (PGW) is an emerging methodology for event-based projections, enabling assessment of the impacts of one or more meteorological parameters over local-scale weather events (Brogli et al., 2019; Fowler, Lenderink, et al., 2021; Moustakis et al., 2021; Prein et al., 2017; Sato et al., 2007; Schär et al., 1996). The PGW methodology imposes a certain climate change, e.g., temperature rise, over the initial and boundary conditions of a regional model, by prescribing the synoptic and larger-scale changes from GCMs, while allowing smaller scale features to develop freely within a downscaled modeled domain in a physically consistent manner. Further, projections of precipitation extremes under global warming scenarios commonly focus on daily resolutions (Donat et al., 2016; O'Gorman, 2015; Pfahl et al., 2017), which hinders the possible impact of short-duration extremes; only recently more studies have directed attention to changes expected over sub-daily or even sub-hourly extremes (Fowler, Ali, et al., 2021; Fowler, Wasko, et al., 2021; Morrison et al., 2019). However, to understand the potential effects of changes in precipitation extremes, not only their changing intensity and frequency are important, but also high-resolution changes in intra-event characteristics, such as the spatiotemporal organization of the storms (Li et al., 2018). This requires high-resolution analysis of many high-impact storms of different synoptic-scale circulations, as there is no guarantee that different HPEs behave the same way (Fowler, Ali, et al., 2021).

The goal of this study is to identify and quantify changes in rainfall patterns during HPEs induced by global warming, and to examine whether a common change emerges over a variety of HPEs. To do so, we exploit the case of the eastern Mediterranean (Sect. 2.1) to simulate a large

number of HPEs using the PGW methodology with a very high spatiotemporal resolution, and explicitly consider space-time patterns of rainfall during the events over durations of 10-min to 24-h.

The paper is organized as follows: Section 2 describes the study region and outlines the modeling strategy and the analyses of rainfall patterns. We first demonstrate the expected changes for a specific HPE case (Sect. 3.1), and then examine changes in rainfall accumulation over a large set of HPEs (Sect. 3.2). Changes in specific rainfall properties are outlined in Sect. 3.2-3.4, with the unique role of the rain area shown in Sect. 3.3.1. Section 4 begins with a discussion of the event-based approach (Sect. 4.1) and continues with an examination of the change in rainfall patterns in future HPEs (Sect. 4.2). Our conclusions are presented in Sect. 5.

2 Study Region, Data, and Methods

2.1 Study Region

The focus here is on the eastern Mediterranean (Fig. 1), which (a) is expected to suffer from a large future decrease in total rainfall (Garfinkel et al., 2020; Giorgi & Lionello, 2008; Zappa et al., 2015), (b) may experience an increase in extreme precipitation occurrence (Alpert et al., 2002; Marra et al., 2021; Samuels et al., 2017), (c) is characterized by the least precipitation per capita in the world (Dirmeyer et al., 2009), and (d) is exposed to large rainfall variability (Morin, 2011). These characteristics result in a large dependency on HPEs, in terms of water resources and vulnerability to natural hazards; therefore, we explore here possible future changes in HPEs in the region, and disassemble them to their distinct hydrometeorological constituents. It is important to note there is currently no CPM with future projections available for the study region.

In the eastern Mediterranean (Fig. 1a), the Mediterranean climate abuts the semiarid to hyperarid climates characterizing the region to the south and east of the Mediterranean Sea. Yearly rainfall amounts drop from >1000 mm in the northern mountains, to <<100 mm at the southeast regions (Fig 1b). Summers are dry, and the rainy season is October to May, with a few rare exceptions in September and June (Yair Goldreich, 2012; Kushnir et al., 2017). The core of the rainy season is December-February (>65% of precipitation). However, the rainy season's midpoint changes from the beginning of January near the Mediterranean Sea to the end of January farther inland (Y. Goldreich, 1994; Yair Goldreich, 1995). This reflects the important contribution of the warm Mediterranean Sea water to building up of Mediterranean Cyclones (MCs), the favorable synoptic condition prevailing during rainy days, generating >90% of all rainfall in the northern, wetter part of the region (Alpert & Shay-EL, 1994; El-Fandy, 1946; Ziv et al., 2006). Other synoptic systems contribute relatively large rain amounts to the interior-desert area mainly during the transitional seasons (Armon et al., 2019; Dayan & Morin, 2006; Kahana et al., 2002), including the more frequent (a) active Red Sea troughs (ARSTs) (Ashbel, 1938; De Vries et al., 2013), occurring mainly in fall, and (b) less frequent disturbances in the Subtropical Jet sometimes termed Tropical Plumes or Active Subtropical Jet (Armon et al., 2018; Dayan & Abramski, 1983; Rubin et al., 2007; Tubi et al., 2017).

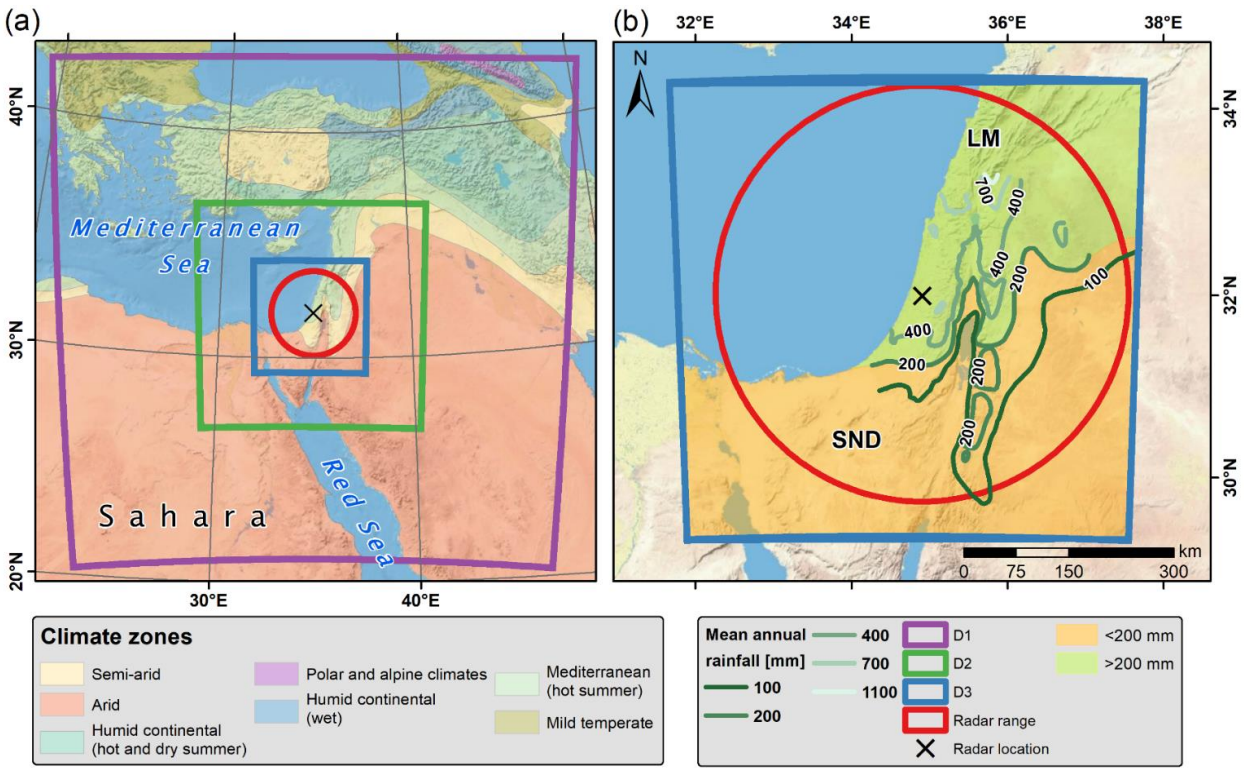

Figure 1. Map of the study area. (a) Köppen-Geiger climate classification of the eastern Mediterranean (Atlas of Israel, 2011), weather research and forecasting (WRF) model domains (D1-D3; Sect. 2.3), and the range of the weather radar used for the identification of events (Sect. 2.2). (b) Mean annual rainfall based on 1960-1990 interpolated rain gauge data (Enzel et al., 2003), the innermost model domain, and the weather radar range. Green and yellow colors, corresponding to drier and wetter than 200 mm yr^{-1}, respectively, roughly mark the extent of the desert and Mediterranean climate regions. SND = Sinai-Negev Desert, LM = Lebanon Mountains.

2.2 HPEs Identification

A collection of carefully selected HPEs was used in this study (Table S1 in the Supporting Information) following Armon et al. (2020) and described here briefly. It consists of 41 HPEs identified based on their magnitude compared to a 24-year rainfall climatology from physically-corrected and gauge-adjusted weather radar rainfall data (Marra & Morin, 2015; Fig. 1b). A HPE was identified when at least a thousand 1-km^2 radar pixels exhibited a rain amount greater than the local 99.5th quantile of the non-zero amounts for multiple durations, thus revealing events which can be considered locally intense. To have a good representation of both short- and long-duration HPEs, this process was repeated for durations of 1-72 h. Events identified as a HPE for more than one duration were merged (Table S1). Return levels of the 99.5th quantile thresholds are roughly 2-10 years. Events were separated by at least 24 h with less than 100 pixels displaying rainfall of more than 0.1 mm, and they span 3.4 ± 1.6 d (mean and standard deviation). This collection of HPEs represents a large variance of synoptic conditions, associated with both MCs (35 events) and ARSTs (six events). A detailed description of the collection of events and their rainfall characteristics is given in Armon et al. (2020).

2.3 WRF Simulations

Each of the 41 HPEs was simulated twice, using version 3.9.1.1 of the weather research and forecasting (WRF) model, at a convection permitting resolution. The first simulation of each event represents the historic conditions during the storm (near the end of the 20th century; sect. 2.3.1). Results of these simulations were previously published (Armon et al., 2020). The second simulation represents a hypothetic storyline in which the same HPE hits the area by the end of the 21st century, when global warming conditions at a representative concentration pathway (RCP) 8.5 prevail in the region (sect. 2.3.2).

2.3.1 Simulation of Historic HPEs

Simulation of historic HPEs was conducted at a configuration suitable for a skillful representation of rainfall patterns in the eastern Mediterranean (Armon et al., 2020; Romine et al., 2013; Rostkier-Edelstein et al., 2014; Schwartz et al., 2015). This configuration includes three two-way nested domains (Fig. 1a; Table S2) in which the innermost domain is simulated at a very high spatial and temporal resolution (1 km^2, 4-8 s). Convective parametrization was used only in the two outer nests, while in the inner nest the resolution is high enough to explicitly represent convection (e.g. Prein et al., 2015). Further details are described in Table S2 and in Armon et al. (2020).

Initial and boundary conditions for the historic simulations are 6-hourly ERA-Interim reanalysis data, at 60 vertical layers with a T255 spectral spatial resolution (~80 km) (Dee et al., 2011). HPEs were simulated starting 24 h before the beginning of the observed rainfall (rounded down to the previous 6 h) and lasted until the end of the HPE (rounded to the following 6 h). The 24 h period before the event is considered a spinup phase, for which we discard the rain fields. This duration is considered long enough to correct spatial heterogeneities arising from the initial conditions (Gómez-Navarro et al., 2019; Picard & Mass, 2017; Warner, 2011: pp 215-216), which is crucial in correcting non-physical properties of the atmosphere, expected to be present in the PGW simulations because of the usage of ensemble mean fields (Shepherd, 2019; Tebaldi & Knutti, 2007) (Sect. 2.3.2). Precipitation outputs for the innermost domain were saved at 10 min intervals.

As was shown by Armon et al. (2020), the total precipitation during most of the HPEs reproduces the structure, location, and the seasonal change of the precipitation's center-of-mass of radar-observed precipitation, albeit with a positive bias. Given that HPEs in the region are characterized by small spatiotemporal scale rain-cells, it is important to note the model's skill is particularly good at its "raw" (1 km^2) resolution for total rain amounts of <25 mm, however, for larger amounts a skillful representation must include a spatial averaging of at least a few tens of square kilometers. The model also well represents areal mean rainfall amounts, for various durations, which are crucial drivers of the hydrological response to precipitation. MC-type HPEs are better simulated compared to ARSTs, which are in general shorter and more local in nature.

2.3.2 Simulation of "Future" HPEs

To simulate the occurrence of the same HPEs in the future we used the "pseudo global warming" (PGW) methodology (Kawase et al., 2009; Rasmussen et al., 2011; Schär et al., 1996). Each of the simulated HPEs was forced with the same input data as the historic events (Sect. 2.3.1) after adding the signal of climate change to the following input variables: surface pressure, skin temperature (including sea surface temperature), and 3D fields of temperature, wind, and

specific humidity. In contrast to homogeneous changes common in the surrogate climate-change methodology (Keller et al., 2018; Schär et al., 1996), 3D spatial heterogeneity in the altered fields used in PGW experiments allows for representation of non-uniform spatial response to global warming (e.g., Rasmussen et al., 2011).

The changes applied over the initial and boundary conditions, for each pixel and timestep (denoted hereon as Δ), were derived from the monthly values (Oct-Apr) of the ensemble mean of 29 models of the Coupled Model Intercomparison Project phase 5 (CMIP5; Table S3) (K. E. Taylor et al., 2012). They were based on the difference in the corresponding parameter values for the end of the 21st century and the end of the 20th century under an RCP 8.5 scenario, as follows:

$$\Delta X_j = \overline{\overline{X}}_J\Big|^{29\,models}_{\mathbf{2074-2099}} - \overline{\overline{X}}_J\Big|^{29\,models}_{\mathbf{1979-2004}}, \quad (1)$$

where X is a specified meteorological variable, defined for the particular month (j) of the HPE occurrence. The double overbar represents the mean of this parameter over the future (2074 to 2099) or historic (1979 to 2004) periods, averaged among the 29 CMIP5 models. Δ fields were linearly interpolated into a common grid, similar to the ERA-Interim horizontal grid (T255) and consisting of 42 levels in the vertical (model top = 10 hPa) for the 3D fields, over the entirety of the outermost domain. The changes applied represent a major warming of the region over the whole troposphere, but specifically over its upper levels. Surface temperature increases on average by 4.3°C. Alongside the warming, is a decrease in the zonal component of wind and an increase of the sea level pressure in the central Mediterranean, as detailed in the Supporting Information Text S1 and Fig S1.

2.4 Analyzed Rainfall Parameters and Statistical Methods

The parameters examined here are based on the 10-min rainfall fields from the innermost domain of both the historic and the "future" (PGW) simulations. Rainfall parameters from the historic and future simulations were compared both through their entire distribution across all events and through an event-based paired comparison (historic-future). To enable comparison between events of different magnitudes, in many instances we normalize the quantity examined to its historic value: $100 \times \frac{\overline{future_i - historic_i}}{\overline{historic_i}}$, where i indicates a specific event for which "future" and "historic" quantities are spatially averaged.

The following rainfall parameters were considered for each event:

(1) Rainfall accumulation for each pixel.

(2) Areal mean rainfall accumulation, which is the average of (1) over the region of interest.

(3) Factors affecting areal mean rainfall accumulation: the value in (2) above can be obtained by integrating rain rates over all rainy pixels and timesteps and divide by the area of the region. Therefore, it is possible to consider three factors affecting the areal mean accumulation:

(a) The mean conditional rain rate is the average of rain rates >0.1 mm h^{-1} over all timesteps and pixels.

(b) The duration of the events is defined here as the time it took the central 90% of rainfall mass to precipitate.

(c) The rain area of the event is the time-average of the area covered by 10-min rain rates >0.1 mm h^{-1} along the event. We also examine the rain area for higher rain rate thresholds in the range of 0.5-100 mm h^{-1}.

(4) Maximal rain rates for durations of 10, 20 and 30 min, 1, 3, 6, 12 and 24 h for each pixel. To diminish the effect of single outlier pixels, the rain field is first smoothed spatially using a 3X3 pixel moving average window.

(5) Regionally maximal rain rates for the same durations as in (4), which are taken as the maximal value from (4) over all pixels in the region.

The analyses above were evaluated both over the entire study region and over four sub-regions (Fig. 1b). These are the Mediterranean Sea area, the land area, and a division of the latter to the area north to the 200 mm isohyet roughly corresponding to the Mediterranean climate zone, and the area south of the 200 mm isohyet roughly corresponding to the desert climate zone.

To analyze changes in the spatial structure of precipitation we compared the spatial autocorrelation structure of the 10-min rain fields whenever these were considered as having convective elements, following Marra and Morin (2018). Convective elements are defined here as spatially connected regions of area ≥3 km^2 with rain rates >10 mm h^{-1} that include at least one pixel with rain rate >25 mm h^{-1}. Following Peleg et al. (2013), the spatial autocorrelation was calculated through fitting a three-parameter exponential function to the 2D spatial autocorrelation field (e.g., Nerini et al., 2017) of each of the convective rain fields as in Eq. 2:

$$r(h) = ae^{-\left(\frac{h}{b}\right)^c}, \quad (2)$$

where h is the lag distance, b, termed the correlation distance, is the distance at which the correlation decreases to $r = ae^{-1}$, a is the nugget (interception) parameter and c is the shape parameter. For each event, the representative parameters of Eq. (2) are the intra-event medians over all convective rain fields. The comparison of the autocorrelation structure between historic and future events is based on the inter-event medians of these representative parameters.

Statistical significance of the changes in *pixel*-based parameters is determined through the paired t-test with 5% significance level. For event-based parameters, statistical significance is declared if both paired t-test and paired Wilcoxon signed-rank tests are statistically significant at the 5% level.

3 Results

To have a better understanding of the changes between "future" (PGW) and historic simulations, we first present an examination of the first HPE in our collection, which exhibits many of the features observed throughout the events. It is followed by the results obtained throughout the HPEs collection.

3.1 Case Study #1

The first HPE in our collection (2-5 Nov 1991) is characterized by the passage of a MC, triggering numerous rain cells crossing the region with a general SW-NE track. These rain cells contributed >100 mm of accumulated rainfall mainly to the north coast and mountainous areas of the study region (Fig. 2a, Movie S1). The areal average rainfall accumulation simulated over the entire domain for the historic event is 21.9 mm. Compared to the historic event, the future event

exhibits a pronounced (-20%) decrease in precipitation with areal average rainfall accumulation summing to 17.5 mm (Fig. 2b-c). The decrease is more pronounced over the land area (-28%) compared to the sea area (-16%), and is similar between the desert and Mediterranean regions of the land area (-29% and -27%, respectively).

In contrast to the decrease in total rain amounts, short duration (10-min) rain rates reveal a more complicated pattern (Fig. 2d). When considering the distribution of all 10-min timesteps and pixels, including those with no-rain (i.e., unconditional rain rates), most of the distribution presents decreased rain rates and only the uppermost quantiles (>99.75%) of future rain rates increase compared to the historic ones. For example, the 99.99% quantile (corresponding to ~1.4 10^4 pixel-timesteps values of 10-min rain rates), is increased by 21% (from 77 mm h^{-1} to 93 mm h^{-1}). However, the decrease in most of the unconditional rain rate quantiles is very much affected by the change in the spatiotemporal coverage of the event, namely the wet-frequency. Conversely, considering the distribution of the rainy pixels and timesteps, i.e., the conditional 10-min rain rate, quantiles of the future HPE are increasing throughout the distribution (Fig. 2d inset). The mean value of the conditional rain rate increases from 2.64 mm h^{-1} for the historic event to 3.43 mm h^{-1} for the future one (+30%).

In addition to the mean conditional rain rate, two other factors affect the areal mean rainfall (Sect. 2.4), the duration and the rain area (Fig. 2e). The duration of the event (Fig. S2a) decreased from 2440 min to 1850 min (-24%) between the historic and future simulations. This reduction reflects a delayed start of the "core" of the rainfall during the passage of the MC, and an earlier termination (Movie S1). The rain area (Fig. 2e) exhibits a major contraction (-38%) between the historic and future simulations, from 31.9 10^3 km^2 (10.5% of the study region) to 19.7 10^3 km^2 (6.5%) in historic and future simulations, respectively. This major decrease in rain area reflects the decrease in the area of precipitating rain cells, seen clearly in Movie S1, as well as in their number. However, it is important to note that we leave for future work a quantitative assessment or tracking of individual rain cells (e.g., Belachsen et al., 2017; Peleg & Morin, 2012). Nevertheless, we did compute the spatial autocorrelation of convective rainfall (Sect. 2.4). The spatial autocorrelation distance is 7 km and 5 km, respectively for the historic and future events (Fig. S2b). In addition, the number of 10-min convective timesteps decreases by 5.1% (from 429 to 407).

In summary, this case study of the first HPE in our collection indicates that, moving from historic to future climates, areal mean rainfall accumulation decreases whereas conditional 10-min rain rates increase. This opposing behavior is caused by the decrease in the duration of the rainfall and even a greater decrease in the rain area, where the latter is probably due to the reduction in the area of precipitating rain cells and possibly in their number. The decrease in duration and in rain area, which means a decrease in wet-frequency, leads also to a decrease in almost all quantiles (except the uppermost ones) of the unconditional rain rate distribution, while the conditional rain rate distribution presents an increase in all quantiles.

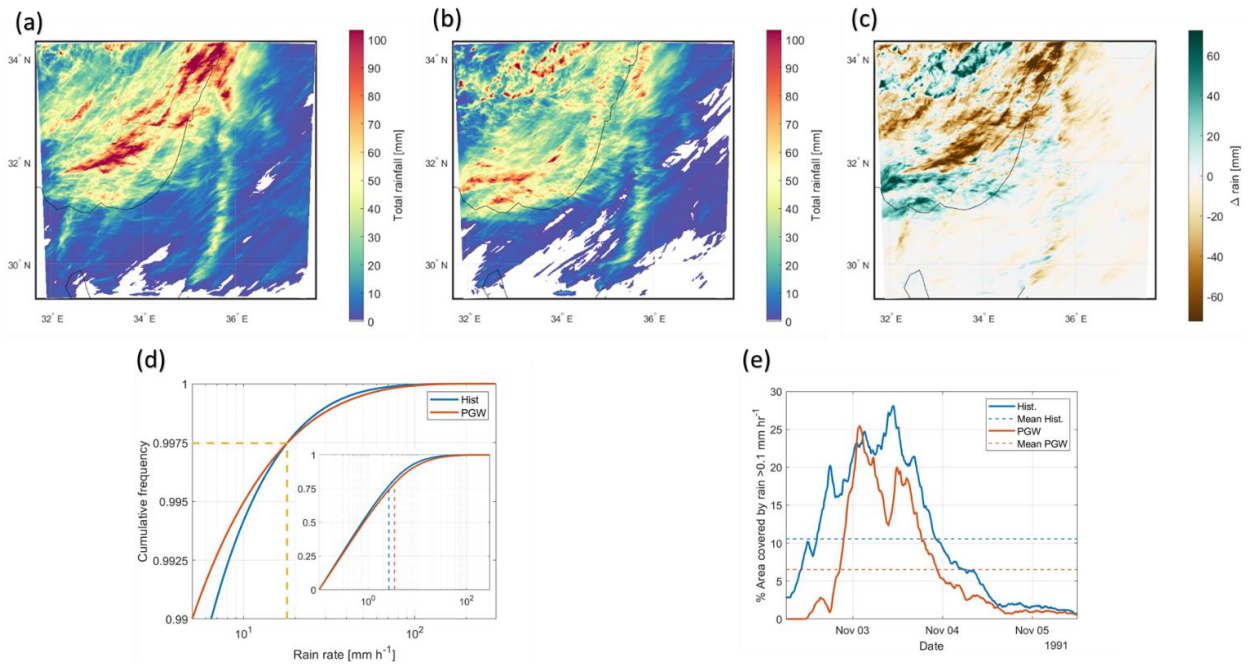

Figure 2. Rainfall in HPE#1 (2-5 Nov 1991). (a) Total rainfall for the historic simulation (see Armon et al. (2020): Fig. 7 for a comparison with precipitation measured by the weather radar). (b) Total rainfall for the future (PGW) simulation. (c) Difference between historic and future simulations (future – historic). (d) Upper 1% quantile of the cumulative frequency curve of unconditional 10-min rain rates throughout the event (i.e., including no-rain intervals and pixels) for the historic (blue line) and future (orange) events. The dashed yellow line marks their intersection. The small inset presents the full cumulative frequency curve of conditional 10-min rain rates (where rain rate >0.1 mm h^{-1}), with mean rain rates in dashed lines. (e) Time series of the areal coverage of rainfall (% of the area covered by rain rate >0.1 mm h^{-1}). Note the larger historic relative to the future unconditional rain rates (up to the 99.75% quantile [marked with yellow dashed line]; panel d) and the rain area (e) while future conditional rain rates are larger throughout the distribution (inset in d and Fig. S2a).

3.2 Decreased Rainfall Accumulation Throughout Events

In general, future simulations show a significant decrease in rainfall accumulation compared with historic simulations (Fig. 3), with a sum of the areal average over all 41 events of 485 mm, compared to 601 mm, respectively (-19%). This decrease is seen throughout the region, with >90% of the area exhibiting decreased rainfall. Given the large variability in rainfall in the region (inter-annual, inter- and intra-event), the fact that 35% of the area shows a significant change in rainfall accumulation highlights the robustness of the results. Out of the portion of pixels showing a statistically significant change, 99.97% exhibit a decrease in total rainfall. In absolute terms, this decrease is most severe in the wetter part of the region (the northern area and the mountains); 1% of pixels show a decrease of ≥618 mm (Fig. 3c). In relative terms, the decrease is most drastic over the Sinai desert and throughout Jordan; 1% of pixels show a decrease of at least 55% (Fig. 3d).

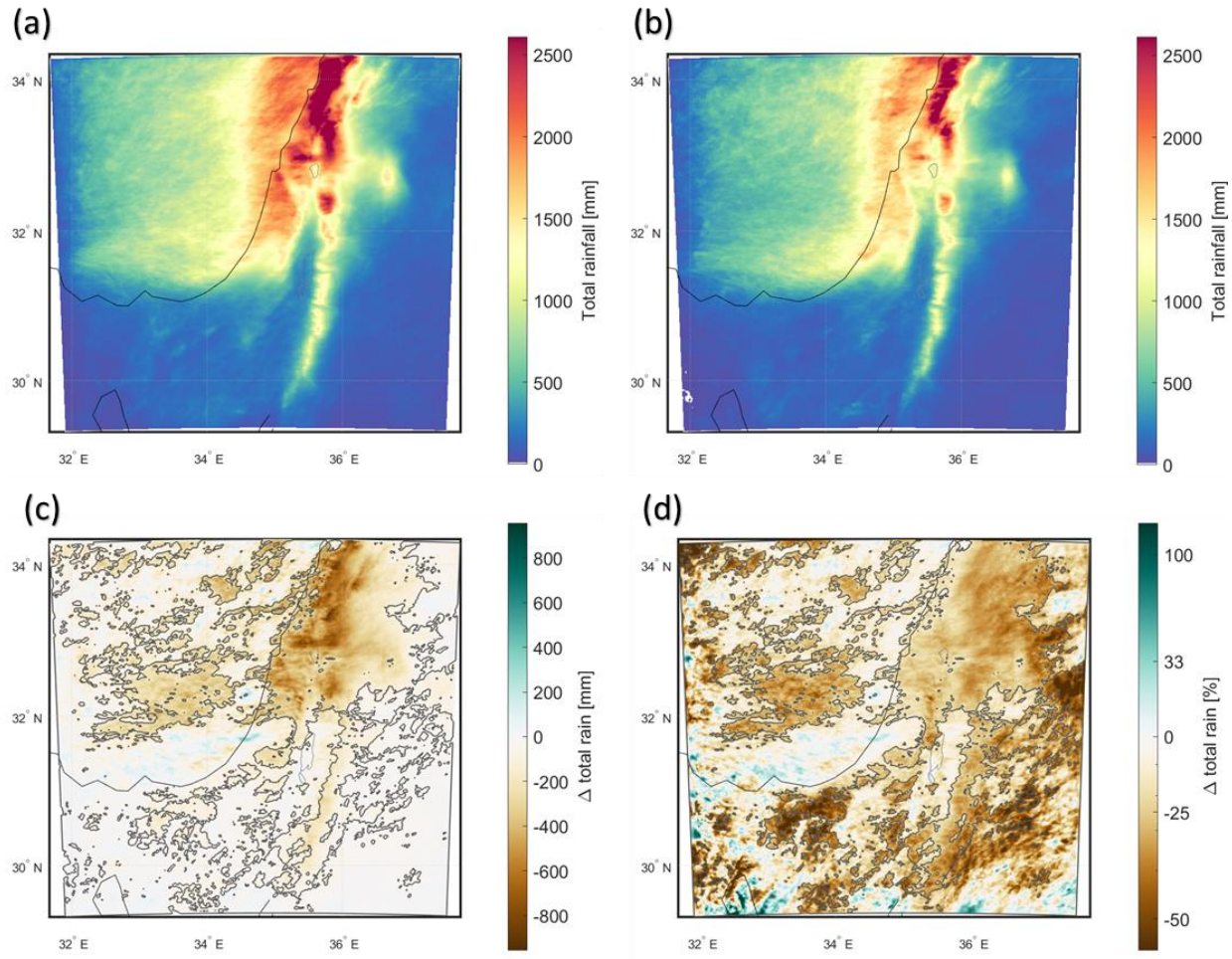

Figure 3. Total rainfall summed over the 41 HPEs historic (a) and future (PGW) simulations. (c) Difference between historic and future simulations (future – historic). Statistically significant differences are demarcated by gray lines. (d) Same as (c) but in relative terms: $(100 \times \frac{future-historic}{historic})$.

The decrease in rainfall accumulation recognized above for the first HPE is preserved among most of the analyzed HPEs. More than 90% of events feature smaller rainfall accumulations in future compared to historic simulations (Fig. 4a, Table 1) with a significant inter-event average decrease of -2.8 mm (equivalent to -30%). Like the first case study, the decrease is more pronounced over land compared to the sea with a significant change of -36% and -26% in average precipitation, respectively. Similarly, 95% and 83% of HPEs were smaller in future compared to historic simulations over land and sea, respectively. The decreased precipitation is significant in each of the sub-regions considered here (Fig. 4b, Fig. S3, Table 1).

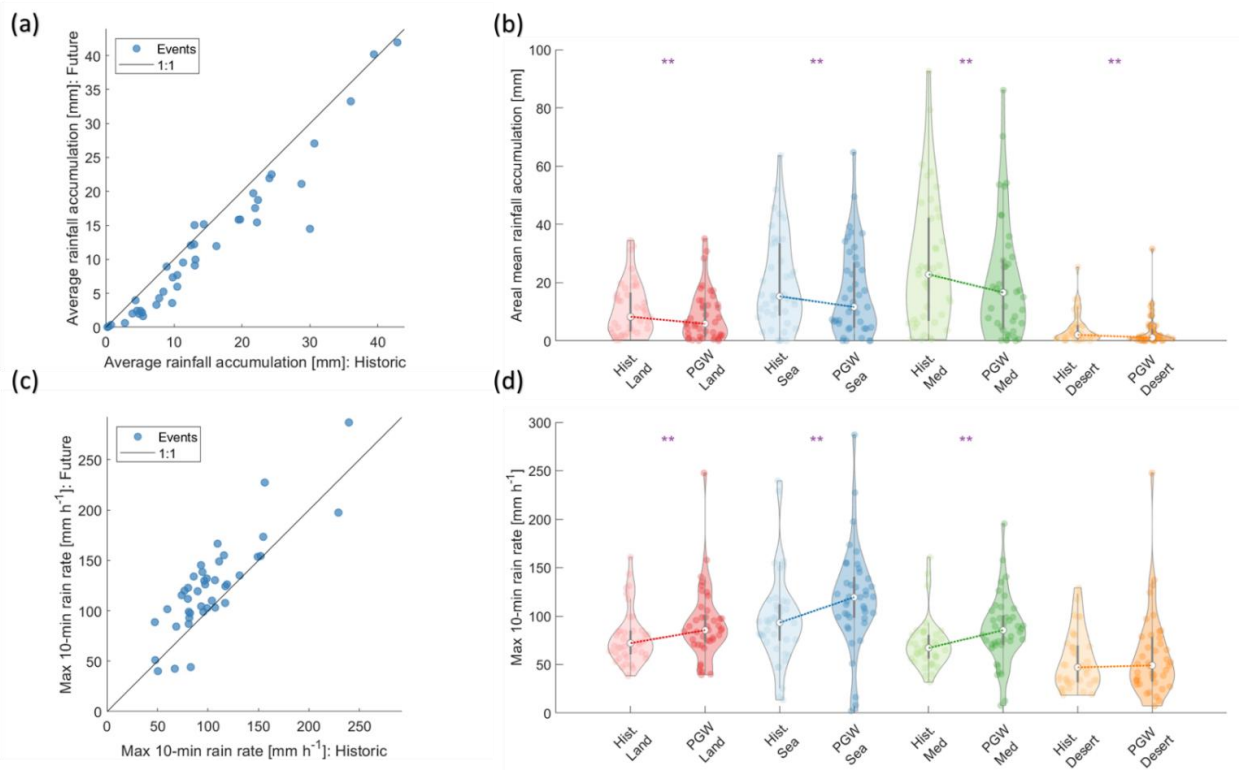

Figure 4. Comparison of future and historic areal mean rainfall accumulation for all 41 HPEs analyzed (a-b, Sect. 3.2), and the regional maximal 10-min rain rates (i.e., along all the pixels in the region and throughout timesteps) (c-d, Sect. 3.4). Scatter plots (a, c) compare the historic (horizontal axis) and future (vertical axis) values. Violin plots (b, d) show the distribution of historic (pale colors) and future (bold colors) quantities for the different sub-regions (Fig. 1b). Each dot along the violin represents a value of one HPE, white dots are median values, and gray boxes are the inter quartile range. The change between medians of historic and future events is marked with dashed lines. Statistically significant differences between the paired-event populations for each region (presented also as scatter plots in Fig. S3 and S7) are marked here with ** (see also Table 1).

Table 1: Changes in rainfall properties between future and historic simulations. Bolded numbers are statistically significant (i.e. on both paired t- and paired Wilcoxon signed-rank tests, Sect. 2.4). Italics are significant on the paired t-test only. The upper value represents the entire region and below are values for each sub-region (land, sea, med=Mediterranean, and des=desert, Fig. 1b).

	Fraction of HPEs exhibiting larger values in future [%]				**Average normalized change:** $\frac{1}{n}\sum_{i=1}^{n}\left(\frac{future_i - historic_i}{historic_i}\right)$ [%]			
Areal average rainfall accumulation	10				**-30**			
	Land	Sea	Med	Des	Land	Sea	Med	Des
	5	17	10	12	**-36**	**-26**	**-34**	**-37**
Regionally max 10-min rain rate	85				**22**			
	Land	Sea	Med	Des	Land	Sea	Med	Des
	80	83	83	63	**18**	**23**	**21**	11
Duration	24				**-9**			
	Land	Sea	Med	Des	Land	Sea	Med	Des
	24	29	24	37	**-8**	**-7**	**-8**	*2*
Rain area	2				**-40**			
	2	2	2	2	**-42**	**-38**	**-41**	**-42**

3.3 Opposing Changes in Rainfall Properties: Increased Conditional Rain Rates, Decreased Duration and Areal Coverage

Changes in the event-based areal mean rainfall accumulation are examined through changes in three rainfall components: mean conditional rain rate, event duration, and rain area (Fig. 5, Fig. S4-S5). The mean conditional rain rate significantly increases with an average change of 15%, and >85% of the events show higher average conditional rain rate in the future compared with the historic simulations. Although there is some correlation between the changes in mean conditional rain rate and total rainfall (Spearman's correlation: $\rho = 0.37$; Fig. S5) increases as large as 47% (event #16) are observed in events with a reduction of the rainfall accumulation. This suggests that the change in the mean conditional rain is rather weakly related to rainfall accumulation.

While mean conditional rain rate is increasing, the duration of events shows a significant negative change (-9%), from a mean of 3290 min to 2980 min, and >75% of the events are longer in historic compared to future simulations (Table 1). The reduction in durations is not, however, a good predictor for the reduction in total rainfall accumulation, with a low, non-significant negative correlation between the two (Fig. S5).

The third component in this analysis, the rain area, reveals the largest relative change out of all three components. It also presents the highest correlation with the change in rainfall accumulation ($\rho = 0.93$; Fig. S5). The rain area is decreased in all but one of the events (>97% of events) with a significant and substantial average decrease (-40%). Events with the lowest

reduction (or even slight increase) in rainfall accumulation are only those in which the reduction in the rain area is relatively small, while events with a large decrease in rainfall accumulation are accompanied by a large decrease in rain area. These results indicate that the factor most heavily related to changes in rainfall accumulation is the rain area.

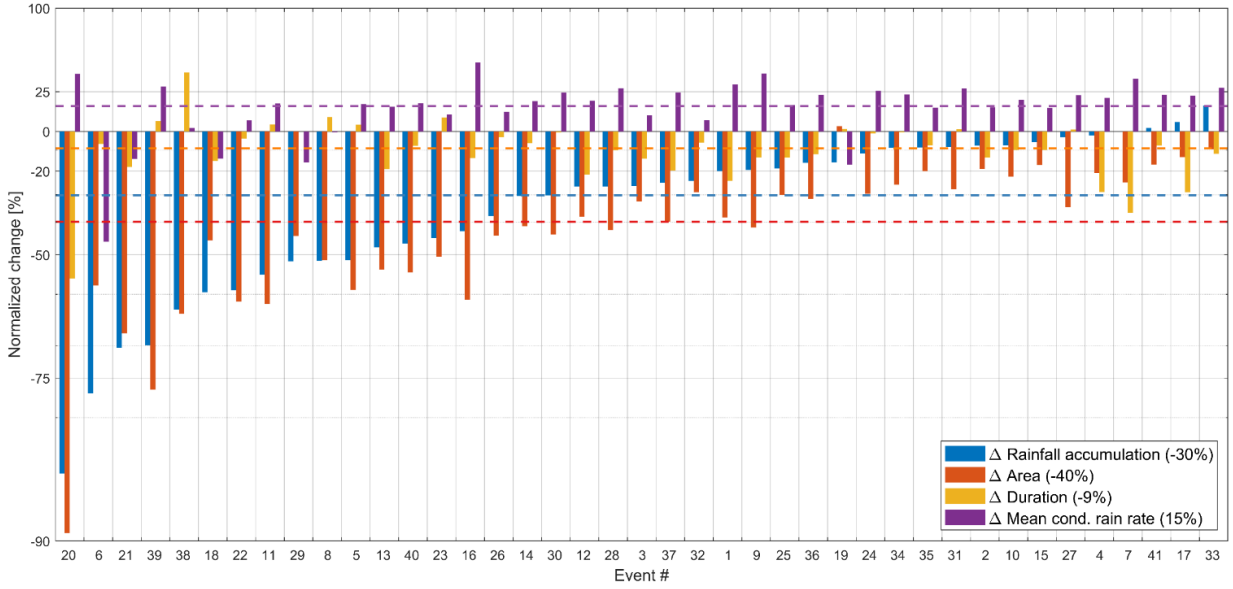

Figure 5. Normalized change between future and historic simulations ($100 \times \frac{future-historic}{historic}$) for the 41 HPEs analyzed. Events are sorted by the change in rainfall accumulation (blue bars). Dashed lines represent average inter-event values (written also inside the legend). The non-normalized changes are shown in Fig. S4. Correlations between the change in rainfall accumulation and the three other parameters are in Fig. S5.

3.3.1 Spatial Concentration of Future Rainstorms

To better understand the changes in the rain area, we examine its changes using a range of rain rate thresholds. Divergent changes in the extent of areas exceeding various rain rates are essential in understanding possible hydrological responses to climate change (Bacchi & Ranzi, 1996; Fowler, Lenderink, et al., 2021; Peleg et al., 2018). Fig. 6a displays the event-average areal rainfall coverage for each HPE with different rain rate thresholds, normalized by the largest coverage for each intensity for both historic and future simulations. The fraction of events with larger areal coverage for each rain rate threshold in historic events, i.e., the relative number of points below the 1:1 line, is displayed in Fig. 6b. The areal coverage of rainfall with relatively low rain rates (0.1-5 mm h^{-1}) is reduced significantly for future compared to historic simulations. The opposite case is true for high rain rates (20-100 mm h^{-1}). This change occurs at rain rates of ~10 mm h^{-1}, where no significant change is documented between rain area above this threshold in historic and in future simulations.

These different trends imply that when compared with historic rainstorms, the total "wet" area in future events is lower, and the storms are more concentrated around the higher rain rates. This conclusion is further strengthened by the change in the autocorrelation pattern of convective rainfall, which demonstrate a much sharper decrease with distance in future compared with

historic simulations and, accordingly, the median of the autocorrelation distance decreases from 8 km to 5 km (Fig. S6).

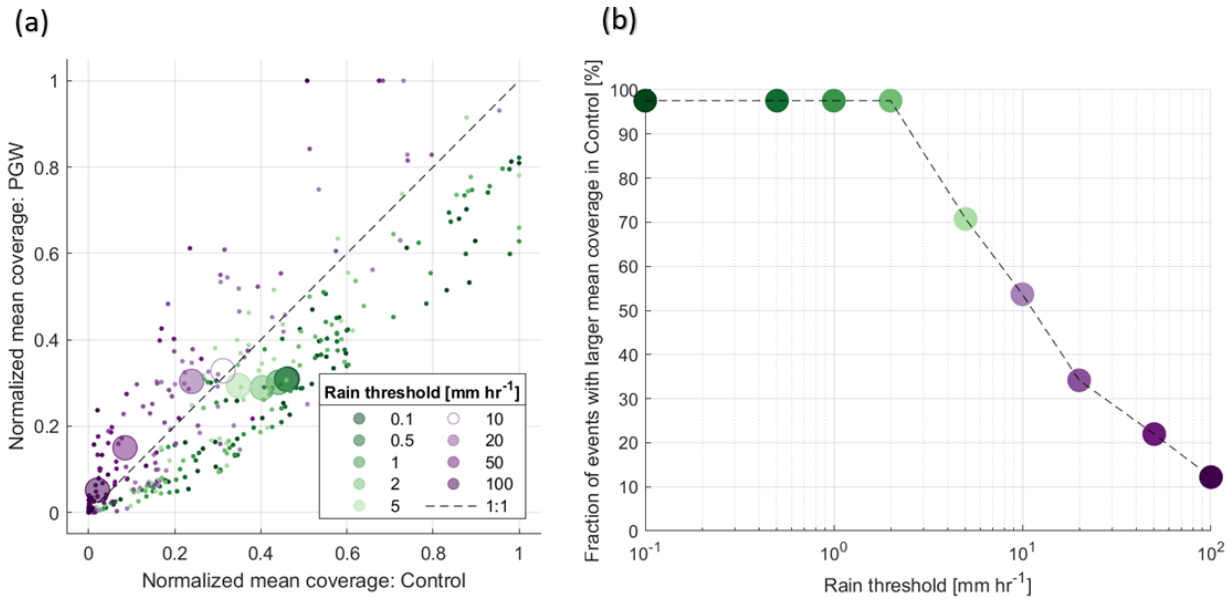

Figure 6. Changes in areal coverage for different rain rate thresholds. (a) Areal mean coverage along each event (small dots) for different rain intensity thresholds (different colors) in historic events (horizontal axis) and future (PGW) events (vertical axis). Values are normalized by the maximal value observed for each rain rate threshold. Average inter-event values are marked with large circles. Filled circles demonstrate statistically significant changes between future and historic values, and one hollow circle shows an insignificant difference. (b) Fraction of events with larger areal coverage in historic compared to future simulations for each of the inspected rain rate thresholds.

3.4 Changes in Extreme Rain Rates for Different Durations

The change in maximal rain rate for each pixel displays different behavior along the study area and between durations. The maps in Fig. 7 show the difference between the inter-event average of the maximum rain rate per event for each pixel, over durations of 10-min to 24-h. For short durations (10-60 min, Fig. 7a-b, Fig. S7), a north-south gradient in maximal rain rates is evident in maximal rain rates. Significant decreases are identified mainly over the southern and eastern desert areas and far into the sea. In contrast, a positive change sub-parallel to the coastline and over Lebanon is present. It is observed mainly a few kilometers offshore and over the mountains at the north of the study region. Over longer durations (a few hours to one day), a larger portion of the region exhibits a significant change in maximal rain intensities (Fig. 7c-d, Fig. S7). This change is almost exclusively negative, focusing over both the desert area and most of the northern land region (excluding the shoreline and the upslopes of the Lebanon Mountains). In relative terms, for the longer durations, almost 25% of the area exhibits a decrease of more than 40% compared with areal-average maximal rain rate in historic events (Fig. S7). It must be noted, however, that the spatial perspective presented in Fig. 7 involves both the increase in rain rates, and the decrease in wet-frequency caused by smaller areal coverage of these intensities and shorter event durations, resulting in a mixture of increased and decreased maximal rain rates.

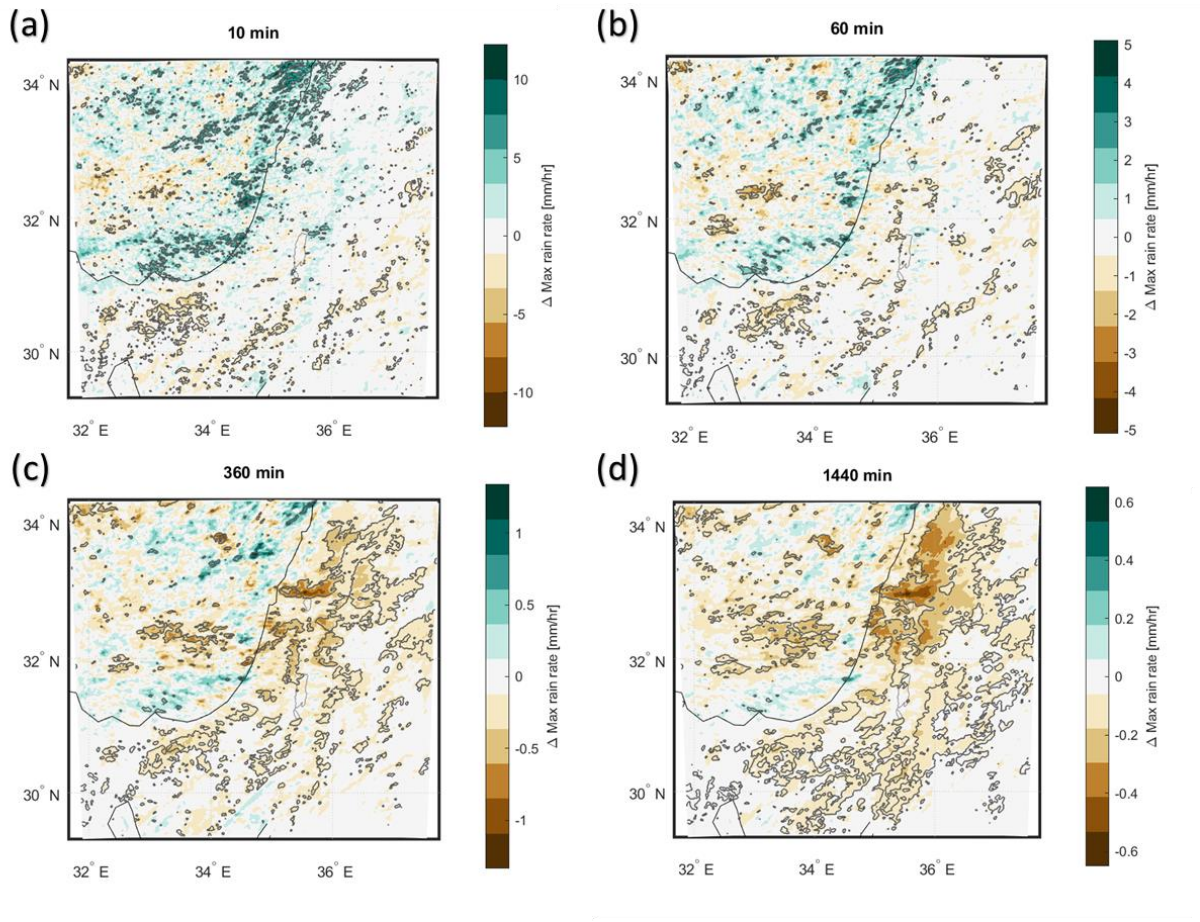

Figure 7. Changes in maximal rain rates averaged over all events for durations of 10-min (a), 1 h (b), 6 h (c) and 24-h (d) between future and historic simulations (future – historic). Statistically significant differences are circumscribed in gray.

In contrast to the decrease in rainfall accumulation, and as exemplified by the first case study (Sect. 3.1), regionally maximal 10-min rain rates (maximum along all pixels and timesteps) in future simulations are significantly higher than in historic simulations (Fig. 4c-d, Table 1) with an average increase of 22%. This conclusion holds for all sub-regions inspected here, except for the desert sub-region, in which the increase (11%) is non-significant (Fig. 4d, Fig. S8, Table 1). Increases of the regionally maximal 10-min rain rates over both the Mediterranean climate and Sea sub-regions are on average >21%, and the increase over land, as a result of the small increase over the desert, is 18%. Furthermore, most of the events (85%) have higher values in future compared to historic simulations and this is rather consistent among the different sub-regions (Table 1). The increase in regionally maximal rain rates between historic and future simulations holds for longer durations as well (Fig. S9).

4 Summary and Discussion

This study shows the changes in rainfall patterns between paired simulations of historic and future HPEs, with the objective of identifying whether common changes in rainfall patterns exist, and characterizing these changes. The collection of objectively identified 41 HPEs was simulated twice, and the results of the two simulations are compared. The first simulation is based on historic conditions, and the second applies expected changes in various meteorological parameters from the RCP 8.5 scenario for the end of the 21st century on top of historic initial and boundary conditions. Selected events represent some of the heaviest precipitation events in the region around the end of the 20th century. Our results, shown first for a case study, and then for the full collection of HPEs, demonstrate the added value of using event-based simulations, and provide high resolution projections of future changes in rainfall patterns, highlighting the importance of changes in specific rainfall constituents, as discussed below.

4.1 Opportunities Gained by the Event-Based Approach and their Implications

Large-scale and long term CPM simulations are becoming increasingly attainable, allowing to better characterize precipitation extremes in future climate scenarios (e.g., Coppola et al., 2020; Kendon et al., 2018). However, there are still difficulties in providing reliable projections of rainfall during HPEs (Kendon et al., 2021); the computational and the power consumption costs of these simulations are huge (Fuhrer et al., 2018; Loft, 2020), and the rarest of extremes are difficult to characterize even in runs extending for many years. Therefore, if the purpose of a study is to identify potential changes in only a subset of the climate, e.g., HPEs, a full-climate run should be used prudently.

Here, using an event-based approach we were able to show plausible impacts of climate change on some of the heaviest rainstorms in the eastern Mediterranean. Furthermore, we show that many "plausible" instances (i.e., individual HPE events) point in the same direction; therefore, the plausible scenario may be considered as the probable scenario. Even if the entire variance of possibilities is not perfectly represented using this method, the emerging similar response enables us to garner insight on "*climate* questions", such as projections of future precipitation patterns, using a *weather* model. We showed that rainfall accumulation under global warming conditions decreases over > 90% of the simulated HPEs and analyzed the properties of rainfall accounting for this decrease. The rain area exhibits the largest and most consistent decrease and is heavily associated with the decrease in rainfall accumulation, while increased conditional rain rate is only weakly related to rainfall accumulation and cannot counteract the decreased rain area.

The simulated change in rainfall patterns can have considerable implications both on water resources and on natural hazards, which can be illuminated if we focus on specific rainstorms. For example, event #8 (1-7 Nov 1994) is an infamous ARST storm in which more than 500 people lost their lives, and extensive floods and damages occurred in Egypt and Israel (Krichak et al., 2000; De Vries et al., 2013). This event shows a substantial reduction in total rainfall under future-simulated conditions (-51%; Fig. 5, Fig. S10). Such a reduction would probably lead to a reduced risk of flash flooding, especially at the northern part of the region. However, while in many places total rainfall decreased in the simulation, few high-intensity rain cells still impacted the Sinai desert (Movie S2), with total rainfall of >100 mm, which would undoubtedly cause substantive floods in this region.

524 HPE #12 (Fig. S11) triggered a major streamflow increase and raised the level of the Sea
525 of Galilee, the largest surficial freshwater reservoir in the region, by 45 cm within a week
526 (compared with <10 cm rise the week before the storm occurred). This rise is equivalent to the
527 yearly industrial consumption of freshwater in Israel at that time (~90 10^6 m^3) and constitutes
528 more than a fifth of the annual water rise of the lake. The simulation of the future event indicates
529 a substantial decrease in total rainfall (-27%). As the hydrological response to decreases in
530 rainfall is non-linear (e.g., Peleg et al., 2014), this would probably lead to an even larger decrease
531 in freshwater recharge with major implications on water resources. While a hydrological
532 simulation of the different events is out of the scope of this paper, we stress that to have better
533 insights about the hydrological response, a comparison of historic and future simulations of
534 specific events through a hydrological model is highly desired.

535 It is important to note that the frequency of events (e.g., Myhre et al., 2019) is not
536 implicitly considered in our simulations. Rain events in the region are projected to have a
537 reduced frequency (~-20%; Hochman et al., 2018; Zappa et al., 2015), and thus, the decreased
538 rainfall we show here for the specific simulated events, may be considered as an underestimation
539 of the projected changes in total precipitation from HPEs accounting for event occurrences.

540 Nevertheless, a minor shortcoming of the PGW methodology is that frequency data is not
541 totally excluded from the applied changes, which arise from the climatology of 25 years of
542 CMIP5 models' simulations. For this reason, changes in specific properties of events should be
543 reflected by the mean climatology. Meaning that if our simulations would constitute a large
544 portion of a 25-yr time interval, they would affect the mean climatology as well. Forty-one
545 HPEs, however, are not a substantial part of the climatological mean of 25 years (~3% of the
546 days in the season we examine [Oct-Apr]), and thus our simulations are not expected to be
547 severely biased by this issue.

548 A potential limitation that this study can be criticized for is the use of a single climate
549 scenario forcing for the PGW and as such it will give only plausible results, rather probable.
550 However, (a) this single scenario is the ensemble mean of CMIP5 models, which can be
551 considered as a best estimate, to date, of large scale future changes, though work currently in
552 progress shows that CMIP6 models generally simulate similar, and if anything more severe,
553 changes to CMIP5 in this region (not shown), (b) we use a collection of many objectively-
554 identified events that constitutes some of the highest magnitude HPEs in the region. Results for
555 this large set of paired-simulations show a similar behavior of different events representing
556 different synoptic-scale conditions. Therefore, we claim that the sign and magnitude of the
557 changes that emerge from these simulations should be considered as a probable projection of
558 HPEs in the region.

559 Indeed, the PGW event-based methodology provides us with projections for HPEs in a
560 warmer climate. However, it must be noted we do not attempt to provide a climatology of HPEs
561 in the future, nor give updated extreme event levels and frequencies. While these can be obtained
562 using a framework which accounts for the frequency of events (Marra et al., 2019), the results
563 we obtain have significance in drawing possible future scenarios for some of the heaviest
564 precipitation events in the region. High resolution rainfall projections can also help improving
565 future predictions in approaches requiring a changed rainfall distribution (e.g., Marra et al.,
566 2021).

4.2 Changes in Rainfall Patterns During Rainstorms

Future rainstorms simulated in this work show quite a difference in rainfall patterns compared to historic rainstorms, mainly being more concentrated in both space and time. Given that the conditional rain rate increases, one might expect an increase in total precipitation during heavy precipitation events, as projected, for example, over Europe (e.g., Y. Chen et al., 2020; Hawcroft et al., 2018; Kendon et al., 2014). However, two other factors, less often addressed, negatively affect total rainfall: the size of the rain area, and the duration of the events. Among these two, we find that the rain area is the main contributor to decreased rainfall accumulation, which decreases, on average, by 40%. Furthermore, the rain area has a high correlation with the changes in rainfall accumulation, while the event duration decreases on average by 9% and has a low correlation with rainfall accumulation changes.

It must be noted, however, that the changes in the rain area are not constant over different rain rates thresholds. The baseline 0.1 mm h^{-1} intensity is a good proxy for the total storm area. Going to larger thresholds, the area represented is a better indicator for the intense "core" of the storm, namely the inner part of convective cells during the storm. In fact, we found an increase in the rain area for thresholds of >10 mm hr^{-1}. This means that, although the total rain area of HPEs shrinks, their cores are getting larger in future simulations. Similar findings were reported by Peleg et al. (2018) using historic radar observations over the eastern Mediterranean and by Wasko et al. (2016) using rain gauges in Australia. Both studies showed that total rain area and the convective core area scale with temperature in opposite directions: total area exhibits a negative scaling, while the area of the convective cores is positively scaled with temperature; this is probably related to an enhanced moisture convergence into the convective cores from the total storm extent. In contrast, results from studies of future extreme precipitation in the Netherlands and in the UK show the area of the storms is expected to increase with global warming (Y. Chen et al., 2020; Lochbihler et al., 2017, 2019), which may indicate a regional dependence in the scaling of the rain area, but this topic should be addressed in future studies (Fowler, Lenderink, et al., 2021).

Since the hydrological response to HPEs is heavily related to space-time precipitation characteristics, the results shown above would have an immense impact on the hydrology of future rainstorms. Larger storm cores, having increased short duration rain rates may increase the risk of urban flooding and short-lived, fast responding flash floods (e.g., Tarasova et al., 2019), as well as soil erosion (e.g., Shmilovitz et al., 2021). However, this effect is expected to be mitigated by the decreased rainfall frequency caused by the shorter storm duration and smaller overall area. Combined, a possible conclusion could be that over the affected (rainy) area, the risk of short-duration natural hazards is higher, while over the entire domain this is uncertain. Yet, a clearer conclusion can be drawn for the detrimental effects of the changes in rainfall patterns over the entire storm through longer-duration processes: mean rain rates and amounts are expected to dramatically decrease. Therefore, the expected hydrological impact would include a further reduction of streamflow and a decline in freshwater resources, which requires immediate address by policy makers.

Two key aspects are missing from the results presented here: a detailed analysis of the meteorological factors affecting the modeled change in rainfall patterns and their scaling with temperature, and a modeling of the hydrological impact of these changes. These two prospective aspects are currently being further studied. We call for a continued use of the PGW methodology

as a relatively easy-to-implement experiment, with results relevant to events of specific interest such as HPEs.

5 Conclusions

Through high-resolution event-based simulations of eastern Mediterranean HPEs in present and future climate, we show that in future: (a) event rainfall accumulations decrease substantially (inter-event average = -30%), throughout the study region, (b) mean conditional rain rate is increased (+15%), (c) event duration is getting shorter (-9%), and (d) rain area becomes dramatically smaller (-40%). The areal coverage for various rain rates shows opposing changes for lower and higher rain rates: it is reduced for low rain rate thresholds, and expanded for high rate thresholds. Thus, rainstorms become more concentrated in future simulations, with convective cores that exhibit shorter autocorrelation distance and higher regionally maximal rain rates (+22%). Furthermore, some increases in local short duration rain rates are seen mostly over the coastal region, but long duration rain rates are decreased throughout the region. The changes found are rather consistent across events, suggesting that these event-based conclusions may actually be probable. Changes in rainfall properties identified here reveal the dominance of the rain area in determining the decrease in total rainfall, with great implications over future hydrological processes.

Acknowledgments, Samples, and Data

The authors thank Y. Shmilovitz and R. Dann for both fruitful discussions and help with coding issues. This research has been supported by the Israel Ministry of Science and Technology (grant no. 61792) and the Israel Water Authority. Shacham radar data for the 41 HPEs are available online (https://doi.org/10.5281/zenodo.5353714). ERA-Interim data were downloaded from the Research Data Archive at the National Center for Atmospheric Research, Computational and Information Systems Laboratory (https://doi.org/10.5065/D6CR5RD9). CMIP5 data were downloaded from the ESGF Node at DKRZ (https://esgf-data.dkrz.de/projects/esgf-dkrz/tou). The WRF namelist.input file can be found in the Supporting Information. FM was supported by the Institute of Atmospheric Sciences and Climate (ISAC) of the National Research Council of Italy (CNR).

References

Alpert, P., & Shay-EL, Y. (1994). The moisture Source for the Winter Cyclones in the Eastern Mediterranean. *Israel Meteorological Research Papers*, *5*, 20–27.

Alpert, P., Ben-Gai, T., Baharad, A., Benjamini, Y., Yekutieli, D., Colacino, M., et al. (2002). The paradoxical increase of Mediterranean extreme daily rainfall in spite of decrease in total values. *Geophysical Research Letters*, *29*(11), 1536. https://doi.org/10.1029/2001GL013554

Armon, M., Dente, E., Smith, J. A., Enzel, Y., & Morin, E. (2018). Synoptic-scale control over modern rainfall and flood patterns in the Levant drylands with implications for past climates. *Journal of Hydrometeorology*, *19*(6), 1077–1096. https://doi.org/10.1175/JHM-D-18-0013.1

Armon, M., Morin, E., & Enzel, Y. (2019). Overview of modern atmospheric patterns

controlling rainfall and floods into the Dead Sea: Implications for the lake's sedimentology and paleohydrology. *Quaternary Science Reviews*, *216*, 58–73. https://doi.org/10.1016/j.quascirev.2019.06.005

Armon, M., Marra, F., Enzel, Y., Rostkier-Edelstein, D., & Morin, E. (2020). Radar-based characterisation of heavy precipitation in the eastern Mediterranean and its representation in a convection-permitting model. *Hydrology and Earth System Sciences*, *24*(3), 1227–1249. https://doi.org/10.5194/hess-24-1227-2020

Ashbel, D. (1938). Great floods in Sinai Peninsula, Palestine, Syria and the Syrian Desert, and the influence of the Red Sea on their formation. *Quarterly Journal of the Royal Meteorological Society*, *64*(277), 635–639.

Bacchi, B., & Ranzi, R. (1996). On the derivation of the areal reduction factor of storms. *Atmospheric Research*, *42*(1–4), 123–135. https://doi.org/10.1016/0169-8095(95)00058-5

Ban, N., Schmidli, J., & Schär, C. (2014). Evaluation of the convection-resolving regional climate modeling approach in decade-long simulations. *Journal of Geophysical Research*, *119*(13), 7889–7907. https://doi.org/10.1002/2014JD021478

Belachsen, I., Marra, F., Peleg, N., & Morin, E. (2017). Convective rainfall in dry climate: relations with synoptic systems and flash-flood generation in the Dead Sea region. *Geophysical Research Abstracts EGU General Assembly*. https://doi.org/10.5194/hess-2017-235

Borga, M., Stoffel, M., Marchi, L., Marra, F., & Jakob, M. (2014). Hydrogeomorphic response to extreme rainfall in headwater systems: Flash floods and debris flows. *Journal of Hydrology*, *518*(PB), 194–205. https://doi.org/10.1016/j.jhydrol.2014.05.022

Brogli, R., Kröner, N., Sørland, S. L., Lüthi, D., & Schär, C. (2019). The role of hadley circulation and lapse-rate changes for the future European summer climate. *Journal of Climate*, *32*(2), 385–404. https://doi.org/10.1175/JCLI-D-18-0431.1

Cannon, A. J., & Innocenti, S. (2019). Projected intensification of sub-daily and daily rainfall extremes in convection-permitting climate model simulations over North America: Implications for future intensity-duration-frequency curves. *Natural Hazards and Earth System Sciences*, *19*(2), 421–440. https://doi.org/10.5194/nhess-19-421-2019

Chan, S. C., Kendon, E. J., Giorgia, B., Elizabeth, F., & Fowler, H. J. (2020). Europe-wide precipitation projections at convection permitting scale with the Unified Model. *Climate Dynamics, (submitted*(0123456789), 1–23. https://doi.org/10.1007/s00382-020-05192-8

Chen, G., Wang, W.-C., Cheng, C.-T., & Hsu, H.-H. (2020). Extreme snow events along the coast of the northeast United States: Potential changes due to global warming. *Journal of Climate*, 1–46. https://doi.org/10.1175/jcli-d-20-0197.1

Chen, J., Wang, Z., Tam, C. Y., Lau, N. C., Lau, D. S. D., & Mok, H. Y. (2020). Impacts of climate change on tropical cyclones and induced storm surges in the Pearl River Delta region using pseudo-global-warming method. *Scientific Reports*, *10*(1), 1–10. https://doi.org/10.1038/s41598-020-58824-8

Chen, Y., Paschalis, A., Kendon, E., Kim, D., & Onof, C. (2020). Changing Spatial Structure of Summer Heavy Rainfall, Using Convection-Permitting Ensemble. *Geophysical Research*

Letters, 1–12. https://doi.org/10.1029/2020gl090903

Coppola, E., Sobolowski, S., Pichelli, E., Raffaele, F., Ahrens, B., Anders, I., et al. (2020). *A first-of-its-kind multi-model convection permitting ensemble for investigating convective phenomena over Europe and the Mediterranean*. *Climate Dynamics* (Vol. 55). https://doi.org/10.1007/s00382-018-4521-8

Crook, J., Klein, C., Folwell, S., Taylor, C. M., Parker, D. J., Stratton, R., & Stein, T. (2019). Assessment of the Representation of West African Storm Lifecycles in Convection-Permitting Simulations. *Earth and Space Science*, *6*(5), 818–835. https://doi.org/10.1029/2018EA000491

Dayan, U., & Abramski, R. (1983). Heavy rain in the Middle East related to unusual jet stream properties. *Bulletin of the American Meteorological Society*, *64*(10), 1138–1140.

Dayan, U., & Morin, E. (2006). Flash flood – producing rainstorms over the Dead Sea: A review. *New Frontiers in Dead Sea Paleoenvironmental Research: Geological Society of America Special Paper*, *401*(04), 53–62. https://doi.org/10.1130/2006.2401(04).

Dayan, U., Lensky, I. M., Ziv, B., & Khain, P. (2021). Atmospheric conditions leading to an exceptional fatal flash flood in the Negev Desert, Israel. *Natural Hazards and Earth System Sciences*, *21*(5), 1583–1597. https://doi.org/10.5194/nhess-21-1583-2021

Dee, D. P., Uppala, S. M., Simmons, A. J., Berrisford, P., Poli, P., Kobayashi, S., et al. (2011). The ERA-Interim reanalysis: configuration and performance of the data assimilation system. *Quarterly Journal of the Royal Meteorological Society*, *137*(656), 553–597. https://doi.org/10.1002/qj.828

Dirmeyer, P. A., Brubaker, K. L., & DelSole, T. (2009). Import and export of atmospheric water vapor between nations. *Journal of Hydrology*, *365*(1–2), 11–22. https://doi.org/10.1016/j.jhydrol.2008.11.016

Donat, M. G., Lowry, A. L., Alexander, L. V., O'Gorman, P. A., & Maher, N. (2016). More extreme precipitation in the world's dry and wet regions. *Nature Climate Change*, *6*(5), 508–513. https://doi.org/10.1038/nclimate2941

El-Fandy, M. G. (1946). Barometric lows of cyprus. *Quarterly Journal of the Royal Meteorological Society*, *72*(314), 291–306. https://doi.org/10.1002/qj.49707231406

Enzel, Y., Bookman (Ken Tor), R., Sharon, D., Gvirtzman, H., Dayan, U., Ziv, B., & Stein, M. (2003). Late Holocene climates of the Near East deduced from Dead Sea level variations and modern regional winter rainfall. *Quaternary Research*, *60*(3), 263–273. https://doi.org/10.1016/j.yqres.2003.07.011

Fatichi, S., Ivanov, V. Y., Paschalis, A., Peleg, N., Molnar, P., Rimkus, S., et al. (2016). Uncertainty partition challenges the predictability of vital details of climate change. *Earth's Future*, *4*(5), 240–251. https://doi.org/10.1002/2015EF000336

Ferreira, R. N. (2021). Cut-Off Lows and Extreme Precipitation in Eastern Spain : Current and Future Climate.

Flaounas, E., Röthlisberger, M., Boettcher, M., Sprenger, M., & Wernli, H. (2021). Extreme wet seasons – their definition and relationship with synoptic-scale weather systems. *Weather and Climate Dynamics*, *2*(1), 71–88. https://doi.org/10.5194/wcd-2-71-2021

Fosser, G., Khodayar, S., & Berg, P. (2014). Benefit of convection permitting climate model simulations in the representation of convective precipitation. *Climate Dynamics*, *44*(1–2), 45–60. https://doi.org/10.1007/s00382-014-2242-1

Fowler, H. J., Lenderink, G., Prein, A. F., Westra, S., Allan, R. P., Ban, N., et al. (2021). Anthropogenic intensification of short-duration rainfall extremes. *Nature Reviews Earth & Environment*, *2*(2), 107–122. https://doi.org/10.1038/s43017-020-00128-6

Fowler, H. J., Wasko, C., & Prein, A. F. (2021). Intensification of short-duration rainfall extremes and implications for flood risk: Current state of the art and future directions. *Philosophical Transactions of the Royal Society A: Mathematical, Physical and Engineering Sciences*, *379*(2195). https://doi.org/10.1098/rsta.2019.0541

Fowler, H. J., Ali, H., Allan, R. P., Ban, N., Barbero, R., Berg, P., et al. (2021). Towards advancing scientific knowledge of climate change impacts on short-duration rainfall extremes. *Philosophical Transactions of the Royal Society A: Mathematical, Physical and Engineering Sciences*, *379*(2195). https://doi.org/10.1098/rsta.2019.0542

Fuhrer, O., Chadha, T., Hoefler, T., Kwasniewski, G., Lapillonne, X., Leutwyler, D., et al. (2018). Near-global climate simulation at 1km resolution: Establishing a performance baseline on 4888 GPUs with COSMO 5.0. *Geoscientific Model Development*, *11*(4), 1665–1681. https://doi.org/10.5194/gmd-11-1665-2018

Garfinkel, C. I., Adam, O., Morin, E., Enzel, Y., Elbaum, E., Bartov, M., et al. (2020). The Role of Zonally Averaged Climate Change in Contributing to Intermodel Spread in CMIP5 Predicted Local Precipitation Changes. *Journal of Climate*, *33*(3), 1141–1154. https://doi.org/10.1175/JCLI-D-19-0232.1

Giorgi, F., & Lionello, P. (2008). Climate change projections for the Mediterranean region. *Global and Planetary Change*, *63*(2–3), 90–104. https://doi.org/10.1016/j.gloplacha.2007.09.005

Goldreich, Y. (1994). The spatial distribution of annual rainfall in Israel - a review. *Theoretical and Applied Climatology*, *50*(1–2), 45–59. https://doi.org/10.1007/BF00864902

Goldreich, Yair. (1995). Temporal variations of rainfall in Israel. *Climate Research*, *5*(2), 167–179. https://doi.org/10.3354/cr005167

Goldreich, Yair. (2012). *The climate of Israel: observation, research and application*. Springer Science & Business Media. https://doi.org/10.1007/978-1-4615-0697-3

Gómez-Navarro, J. J., Raible, C. C., García-Valero, J. A., Messmer, M., Montávez, J. P., & Martius, O. (2019). Event selection for dynamical downscaling: a neural network approach for physically-constrained precipitation events. *Climate Dynamics*. https://doi.org/10.1007/s00382-019-04818-w

Gutmann, E. D., Rasmussen, R. M., Liu, C., Ikeda, K., Bruyere, C. L., Done, J. M., et al. (2018). Changes in hurricanes from a 13-Yr convection-permitting pseudo- global warming simulation. *Journal of Climate*, *31*(9), 3643–3657. https://doi.org/10.1175/JCLI-D-17-0391.1

Hawcroft, M., Walsh, E., Hodges, K., & Zappa, G. (2018). Significantly increased extreme precipitation expected in Europe and North America from extratropical cyclones.

Environmental Research Letters, *13*(12). https://doi.org/10.1088/1748-9326/aaed59

Hochman, A., Harpaz, T., Saaroni, H., & Alpert, P. (2018). The seasons' length in 21st century CMIP5 projections over the eastern Mediterranean. *International Journal of Climatology*, (December 2017), 1–11. https://doi.org/10.1002/joc.5448

Israel, A. of. (2011). *The new Atlas of Israel: the national atlas*. Jerusalem: Survey of Israel ; The Hebrew University of Jerusalem.

Kahana, R., Ziv, B., Enzel, Y., & Dayan, U. (2002). Synoptic climatology of major floods in the Negev Desert, Israel. *International Journal of Climatology*, *22*(7), 867–882. https://doi.org/10.1002/joc.766

Kawase, H., Yoshikane, T., Hara, M., Kimura, F., Yasunari, T., Ailikun, B., et al. (2009). Intermodel variability of future changes in the Baiu rainband estimated by the pseudo global warming downscaling method. *Journal of Geophysical Research Atmospheres*, *114*(24), 1–14. https://doi.org/10.1029/2009JD011803

Keller, M., Kröner, N., Fuhrer, O., Lüthi, D., Schmidli, J., Stengel, M., et al. (2018). The sensitivity of alpine summer convection to surrogate climate change: An intercomparison between convection-parameterizing and convection-resolving models. *Atmospheric Chemistry and Physics*, *18*(8), 5253–5264. https://doi.org/10.5194/acp-18-5253-2018

Kendon, E. J., Roberts, N. M., Fowler, H. J., Roberts, M. J., Chan, S. C., & Senior, C. A. (2014). Heavier summer downpours with climate change revealed by weather forecast resolution model. *Nature Climate Change*, *4*(7), 570–576. https://doi.org/10.1038/nclimate2258

Kendon, E. J., Blenkinsop, S., & Fowler, H. J. (2018). When will we detect changes in short-duration precipitation extremes? *Journal of Climate*, *31*(7), 2945–2964. https://doi.org/10.1175/JCLI-D-17-0435.1

Kendon, E. J., Prein, A. F., Senior, C. A., & Stirling, A. (2021). Challenges and outlook for convection-permitting climate modelling. *Philosophical Transactions of the Royal Society A: Mathematical, Physical and Engineering Sciences*. https://doi.org/10.1098/rsta.2019.0547

Krichak, S. O., Tsidulko, M., & Alpert, P. (2000). November 2, 1994, severe storms in the southeastern Mediterranean. *Atmospheric Research*, *53*(1–3), 45–62. https://doi.org/10.1016/S0169-8095(99)00045-9

Kushnir, Y., Dayan, U., Ziv, B., Morin, E., & Enzel, Y. (2017). Climate of the Levant: Phenomena and Mechanisms. In Y. Enzel & B.-Y. Ofer (Eds.), *Quaternary of the Levant: Environments, Climate Change, and Humans* (pp. 31–44). Cambridge, UK: Cambridge University Press.

Li, J., Wasko, C., Johnson, F., Evans, J. P., & Sharma, A. (2018). Can Regional Climate Modeling Capture the Observed Changes in Spatial Organization of Extreme Storms at Higher Temperatures? *Geophysical Research Letters*, *45*(9), 4475–4484. https://doi.org/10.1029/2018GL077716

Lochbihler, K., Lenderink, G., & Siebesma, A. P. (2017). The spatial extent of rainfall events and its relation to precipitation scaling. *Geophysical Research Letters*, *44*(16), 8629–8636. https://doi.org/10.1002/2017GL074857

Lochbihler, K., Lenderink, G., & Siebesma, A. P. (2019). Response of Extreme Precipitating Cell Structures to Atmospheric Warming. *Journal of Geophysical Research: Atmospheres*, *124*(13), 6904–6918. https://doi.org/10.1029/2018JD029954

Loft, R. (2020). Earth system modeling must become more energy efficient. *Eos*. https://doi.org/10.1029/2020EO147051

Marra, F., & Morin, E. (2015). Use of radar QPE for the derivation of Intensity–Duration–Frequency curves in a range of climatic regimes. *Journal of Hydrology*, *531*, 427–440. https://doi.org/10.1016/j.jhydrol.2015.08.064

Marra, F., & Morin, E. (2018). Autocorrelation structure of convective rainfall in semiarid-arid climate derived from high-resolution X-Band radar estimates. *Atmospheric Research*, *200*(September 2017), 126–138. https://doi.org/10.1016/j.atmosres.2017.09.020

Marra, F., Zoccatelli, D., Armon, M., & Morin, E. (2019). A simplified MEV formulation to model extremes emerging from multiple nonstationary underlying processes. *Advances in Water Resources*, *127*, 280–290. https://doi.org/10.1016/j.advwatres.2019.04.002

Marra, F., Armon, M., Adam, O., Zoccatelli, D., Gazal, O., Garfinkel, C. I., et al. (2021). Towards narrowing uncertainty in future projections of local extreme precipitation. *Geophysical Research Letters*, *Accepted*.

Meredith, E. P., Ulbrich, U., & Rust, H. W. (2020). Subhourly rainfall in a convection-permitting model. *Environmental Research Letters*, *15*(3). https://doi.org/10.1088/1748-9326/ab6787

Morin, E. (2011). To know what we cannot know: Global mapping of minimal detectable absolute trends in annual precipitation. *Water Resources Research*, *47*(7), 1–9. https://doi.org/10.1029/2010WR009798

Morrison, A., Villarini, G., Zhang, W., & Scoccimarro, E. (2019). Projected changes in extreme precipitation at sub-daily and daily time scales. *Global and Planetary Change*, *182*(May), 103004. https://doi.org/10.1016/j.gloplacha.2019.103004

Moustakis, Y., Papalexiou, S. M., Onof, C. J., & Paschalis, A. (2021). Seasonality, Intensity, and Duration of Rainfall Extremes Change in a Warmer Climate. *Earth's Future*, *9*(3), 1–15. https://doi.org/10.1029/2020EF001824

Myhre, G., Alterskjær, K., Stjern, C. W., Hodnebrog, Marelle, L., Samset, B. H., et al. (2019). Frequency of extreme precipitation increases extensively with event rareness under global warming. *Scientific Reports*, *9*(1), 1–10. https://doi.org/10.1038/s41598-019-52277-4

Nasta, P., Adane, Z., Lock, N., Houston, A., & Gates, J. B. (2018). Links between episodic groundwater recharge rates and rainfall events classified according to stratiform-convective storm scoring: A plot-scale study in eastern Nebraska. *Agricultural and Forest Meteorology*, *259*(February), 154–161. https://doi.org/10.1016/j.agrformet.2018.05.003

Nerini, D., Besic, N., Sideris, I., Germann, U., & Foresti, L. (2017). A non-stationary stochastic ensemble generator for radar rainfall fields based on the short-space Fourier transform. *Hydrology and Earth System Sciences*, *21*(6), 2777–2797. https://doi.org/10.5194/hess-21-2777-2017

O'Gorman, P. A. (2015). Precipitation Extremes Under Climate Change. *Current Climate Change Reports*, *1*(2), 49–59. https://doi.org/10.1007/s40641-015-0009-3

Peleg, N., & Morin, E. (2012). Convective rain cells: Radar-derived spatiotemporal characteristics and synoptic patterns over the eastern Mediterranean. *Journal of Geophysical Research: Atmospheres*, *117*(15), 1–17. https://doi.org/10.1029/2011JD017353

Peleg, N., Ben-Asher, M., & Morin, E. (2013). Radar subpixel-scale rainfall variability and uncertainty: Lessons learned from observations of a dense rain-gauge network. *Hydrology and Earth System Sciences*, *17*(6), 2195–2208. https://doi.org/10.5194/hess-17-2195-2013

Peleg, N., Bartov, M., & Morin, E. (2014). CMIP5-predicted climate shifts over the East Mediterranean: Implications for the transition region between Mediterranean and semi-arid climates. *International Journal of Climatology*, *2153*(July 2014), 2144–2153. https://doi.org/10.1002/joc.4114

Peleg, N., Marra, F., Fatichi, S., Molnar, P., Morin, E., Sharma, A., & Burlando, P. (2018). Intensification of convective rain cells at warmer temperatures observed from high-resolution weather radar data. *Journal of Hydrometeorology*, JHM-D-17-0158.1. https://doi.org/10.1175/JHM-D-17-0158.1

Pfahl, S., O'Gorman, P. A., & Fischer, E. M. (2017). Understanding the regional pattern of projected future changes in extreme precipitation. *Nature Climate Change*, *7*(6), 423–427. https://doi.org/10.1038/nclimate3287

Picard, L., & Mass, C. (2017). The sensitivity of orographic precipitation to flow direction: An idealized modeling approach. *Journal of Hydrometeorology*, *18*(6), 1673–1688. https://doi.org/10.1175/JHM-D-16-0209.1

Pichelli, E., Coppola, E., Sobolowski, S., Ban, N., Giorgi, F., Stocchi, P., et al. (2021). The first multi-model ensemble of regional climate simulations at kilometer-scale resolution part 2: historical and future simulations of precipitation. *Climate Dynamics*, *56*(11–12), 3581–3602. https://doi.org/10.1007/s00382-021-05657-4

Poujol, B., Prein, A. F., & Newman, A. J. (2020). Kilometer-scale modeling projects a tripling of Alaskan convective storms in future climate. *Climate Dynamics*, (0123456789). https://doi.org/10.1007/s00382-020-05466-1

Prein, A. F., Langhans, W., Fosser, G., Ferrone, A., Ban, N., Goergen, K., et al. (2015). A review on regional convection-permitting climate modeling: Demonstrations, prospects, and challenges. *Reviews of Geophysics*, *53*(2), 323–361. https://doi.org/10.1002/2014RG000475

Prein, A. F., Rasmussen, R. M., Ikeda, K., Liu, C., Clark, M. P., & Holland, G. J. (2017). The future intensification of hourly precipitation extremes. *Nature Climate Change*, *7*(1), 48–52. https://doi.org/10.1038/nclimate3168

Rasmussen, R., Liu, C., Ikeda, K., Gochis, D., Yates, D., Chen, F., et al. (2011). High-resolution coupled climate runoff simulations of seasonal snowfall over Colorado: A process study of current and warmer climate. *Journal of Climate*, *24*(12), 3015–3048. https://doi.org/10.1175/2010JCLI3985.1

Raveh-Rubin, S., & Wernli, H. (2016). Large-scale wind and precipitation extremes in the Mediterranean: dynamical aspects of five selected cyclone events. *Quarterly Journal of the Royal Meteorological Society*, *142*(701), 3097–3114. https://doi.org/10.1002/qj.2891

Rinat, Y., Marra, F., Armon, M., Metzger, A., Levi, Y., Khain, P., et al. (2020).

Hydrometeorological analysis and forecasting of a 3-day flash-flood-triggering desert rainstorm. *Natural Hazards and Earth System Sciences Discussions*, *2020*, 1–35. https://doi.org/10.5194/nhess-2020-189

Romine, G. S., Schwartz, C. S., Snyder, C., Anderson, J. L., & Weisman, M. L. (2013). Model Bias in a Continuously Cycled Assimilation System and Its Influence on Convection-Permitting Forecasts. *Monthly Weather Review*, *141*(4), 1263–1284. https://doi.org/10.1175/MWR-D-12-00112.1

Rostkier-Edelstein, D., Liu, Y., Wu, W., Kunin, P., Givati, A., & Ge, M. (2014). Towards a high-resolution climatography of seasonal precipitation over Israel. *International Journal of Climatology*, *34*(6), 1964–1979. https://doi.org/10.1002/joc.3814

Rubin, S., Ziv, B., & Paldor, N. (2007). Tropical Plumes over Eastern North Africa as a Source of Rain in the Middle East. *Monthly Weather Review*, *135*(12), 4135–4148. https://doi.org/10.1175/2007MWR1919.1

Samuels, R., Rimmer, A., & Alpert, P. (2009). Effect of extreme rainfall events on the water resources of the Jordan River. *Journal of Hydrology*, *375*(3–4), 513–523. https://doi.org/10.1016/j.jhydrol.2009.07.001

Samuels, R., Hochman, A., Baharad, A., Givati, A., Levi, Y., Yosef, Y., et al. (2017). Evaluation and projection of extreme precipitation indices in the Eastern Mediterranean based on CMIP5 multi-model ensemble. *International Journal of Climatology*. https://doi.org/10.1002/joc.5334

Sato, T., Kimura, F., & Kitoh, A. (2007). Projection of global warming onto regional precipitation over Mongolia using a regional climate model. *Journal of Hydrology*, *333*(1), 144–154. https://doi.org/10.1016/j.jhydrol.2006.07.023

Schär, C., Frei, C., Lüthi, D., & Davies, H. C. (1996). Surrogate climate-change scenarios for regional climate models. *Geophysical Research Letters*, *23*(6), 669–672. https://doi.org/10.1029/96GL00265

Schwartz, C. S., Romine, G. S., Sobash, R. A., Fossell, K. R., & Weisman, M. L. (2015). NCAR's Experimental Real-Time Convection-Allowing Ensemble Prediction System. *Weather and Forecasting*, *30*(6), 1645–1654. https://doi.org/10.1175/WAF-D-15-0103.1

Shepherd, T. G. (2014). Atmospheric circulation as a source of uncertainty in climate change projections. *Nature Geoscience*, *7*(10), 703–708. https://doi.org/10.1038/NGEO2253

Shepherd, T. G. (2019). Storyline approach to the construction of regional climate change information. *Proceedings of the Royal Society A: Mathematical, Physical and Engineering Sciences*, *475*(2225). https://doi.org/10.1098/rspa.2019.0013

Shmilovitz, Y., Marra, F., Wei, H., Argaman, E., Nearing, M., Goodrich, D., et al. (2021). Frequency analysis of storm-scale soil erosion and characterization of extreme erosive events by linking the DWEPP model and a stochastic rainfall generator. *Science of the Total Environment*, *787*, 147609. https://doi.org/10.1016/j.scitotenv.2021.147609

Sillmann, J., Shepherd, T. G., van den Hurk, B., Hazeleger, W., Martius, O., Slingo, J., & Zscheischler, J. (2021). Event-Based Storylines to Address Climate Risk. *Earth's Future*, *9*(2), 1–6. https://doi.org/10.1029/2020EF001783

939 Tarasova, L., Merz, R., Kiss, A., Basso, S., Blöschl, G., Merz, B., et al. (2019). Causative
940 classification of river flood events. *WIREs Water*, *6*(4), 1–23.
941 https://doi.org/10.1002/wat2.1353

942 Taylor, K. E., Stouffer, R. J., & Meehl, G. A. (2012). An overview of CMIP5 and the experiment
943 design. *Bulletin of the American Meteorological Society*. https://doi.org/10.1175/BAMS-D-
944 11-00094.1

945 Taylor, R. G., Todd, M. C., Kongola, L., Maurice, L., Nahozya, E., Sanga, H., & Macdonald, A.
946 M. (2013). Evidence of the dependence of groundwater resources on extreme rainfall in
947 East Africa. *Nature Climate Change*, *3*(4), 374–378. https://doi.org/10.1038/nclimate1731

948 Tebaldi, C., & Knutti, R. (2007). The use of the multi-model ensemble in probabilistic climate
949 projections. *Philosophical Transactions of the Royal Society A: Mathematical, Physical and*
950 *Engineering Sciences*, *365*(1857), 2053–2075. https://doi.org/10.1098/rsta.2007.2076

951 Trenberth, K. E., Fasullo, J. T., & Shepherd, T. G. (2015). Attribution of climate extreme events.
952 *Nature Climate Change*, *5*(8), 725–730. https://doi.org/10.1038/nclimate2657

953 Tubi, A., Dayan, U., & Lensky, I. M. (2017). Moisture transport by tropical plumes over the
954 Middle East: a 30-year climatology. *Quarterly Journal of the Royal Meteorological Society*,
955 *143*(709), 3165–3176. https://doi.org/10.1002/qj.3170

956 De Vries, A. J., Tyrlis, E., Edry, D., Krichak, S. O., Steil, B., & Lelieveld, J. (2013). Extreme
957 precipitation events in the Middle East: Dynamics of the Active Red Sea Trough. *Journal of*
958 *Geophysical Research: Atmospheres*, *118*(13), 7087–7108.
959 https://doi.org/10.1002/jgrd.50569

960 Warner, T. T. (2011). *Numerical Weather and Climate Prediction*.
961 https://doi.org/10.1017/CBO9780511763243

962 Wasko, C., Sharma, A., & Westra, S. (2016). Reduced spatial extent of extreme storms at higher
963 temperatures. *Geophysical Research Letters*, *43*(8), 4026–4032.
964 https://doi.org/10.1002/2016GL068509

965 Westra, S., Fowler, H. J., Evans, J. P., Alexander, L. V., Berg, P., Johnson, F., et al. (2014).
966 Future changes to the intensity and frequency of short-duration extreme rainfall. *Reviews of*
967 *Geophysics*, *52*, 522–555. https://doi.org/10.1002/2014RG000464

968 Zappa, G., Hawcroft, M. K., Shaffrey, L., Black, E., & Brayshaw, D. J. (2015). Extratropical
969 cyclones and the projected decline of winter Mediterranean precipitation in the CMIP5
970 models. *Climate Dynamics*, *45*(7–8), 1727–1738. https://doi.org/10.1007/s00382-014-2426-
971 8

972 Ziv, B., Dayan, U., Kushnir, Y., Roth, C., & Enzel, Y. (2006). Regional and global atmospheric
973 patterns governing rainfall in the southern Levant. *International Journal of Climatology*,
974 *26*(1), 55–73. https://doi.org/10.1002/joc.1238

975

Earth's Future

Supporting Information for

Reduced rainfall in future heavy precipitation events related to contracted rainy area despite increased rain rate

Moshe Armon[1], Francesco Marra[2], Yehouda Enzel[1], Dorita Rostkier-Edelstein[1,3], Chaim I. Garfinkel[1], Ori Adam[1], Uri Dayan[4], Efrat Morin[1]

[1]Fredy and Nadine Herrmann Institute of Earth Sciences, the Hebrew University of Jerusalem, Jerusalem, 9190401, Israel

[2]National Research Council of Italy, Institute of Atmospheric Sciences and Climate, CNR-ISAC, Bologna 40129, Italy

[3]Department of Environmental Physics, Environmental Sciences Division, IIBR, Ness-Ziona 7410001, Israel

[4]Department of Geography, the Hebrew University of Jerusalem, Jerusalem, 9190401, Israel

Contents of this file

Additional Supporting Information (Files uploaded separately)

Text S1. Brief analysis of the climate change applied for PGW simulations

The changes applied, under the RCP 8.5 scenario, represent a major warming of the region. At the ground level a larger temperature increase is seen over land than over the sea with local maxima over the Arabian Peninsula and north-western Asia (Fig. S1a). The warming peaks at the upper troposphere (~300 hPa), where maximum values are near the equator, and is stronger in fall compared to spring (Fig. S1b-c). It is interesting to note that the warming in the upper troposphere is enhanced during fall, which may increase the static stability compared to winter and spring. The pattern of sea level pressure resembles the surface temperature change (with an opposite sign) and exhibits a maximum over the central Mediterranean, and a minimum at the Arabian Peninsula and north-western Asia, implying a decreased frequency of MCs, or a general decrease in sea-land pressure gradient. These changes are in concert with previous studies (e.g., Giorgi and Lionello, 2008; Seager et al., 2019; Tuel et al., 2021; Tuel and Eltahir, 2020). The moisture field is only slightly increased over the Mediterranean region, with larger increases in fall than in spring, and farther to the south in equatorial Africa (Fig. S1b,d). Combined with decreased zonal wind at both the lower and the upper tropopause, this suggests a decrease in moisture flux into the eastern Mediterranean.

Table S1: Heavy precipitation events (HPEs) analysed in this study. Further details on the identification of events are described in Armon et al. (2020). Durations for which each of the HPEs were identified are marked with and X.

HPE #	Start time*	End time*	Synoptic classification[#]	HPE duration [h]						
				1	3	6	12	24	48	72
1	2-11-1991 9:00	5-11-1991 9:00	MC	X	X	X	X	X	X	X
2	22-2-1992 8:00	27-2-1992 21:00	MC						X	X
3	23-11-1992 9:00	26-11-1992 7:00	MC	X	X	X	X			
4	12-12-1992 14:00	18-12-1992 13:00	MC	X	X	X	X	X	X	X
5	31-3-1993 9:00	2-4-1993 2:00	ARST			X				
6	21-12-1993 12:00	23-12-1993 15:00	ARST						X	
7	21-2-1994 19:00	25-2-1994 0:00	MC		X	X	X			
8	1-11-1994 15:00	7-11-1994 13:00	ARST	X	X	X	X	X	X	X
9	14-11-1994 1:00	18-11-1994 5:00	MC	X	X	X	X	X	X	X
10	15-12-1994 12:00	20-12-1994 21:00	MC	X	X			X	X	X
11	28-12-1994 10:00	31-12-1994 23:00	MC			X				
12	4-2-1995 8:00	9-2-1995 10:00	MC					X	X	X
13	1-11-1995 11:00	3-11-1995 14:00	MC	X	X					
14	7-11-1995 10:00	10-11-1995 17:00	MC							X
15	6-3-1996 13:00	8-3-1996 4:00	MC		X	X	X	X	X	
16	11-12-1996 14:00	14-12-1996 15:00	ARST	X	X	X	X	X	X	X
17	13-1-1997 11:00	17-1-1997 7:00	MC	X	X	X	X	X	X	X
18	3-3-1997 6:00	4-3-1997 16:00	MC	X	X	X	X			
19	19-10-1997 11:00	20-10-1997 10:00	MC		X	X	X			
20	25-11-1997 10:00	27-11-1997 9:00	ARST		X	X	X	X		
21	4-4-1998 4:00	4-4-1998 17:00	MC			X	X			
22	28-12-1998 6:00	31-12-1998 21:00	MC	X	X	X	X	X		
23	13-12-1999 6:00	15-12-1999 8:00	MC	X	X	X	X			
24	18-1-2000 6:00	24-1-2000 2:00	MC		X	X	X	X	X	X
25	25-1-2000 15:00	28-1-2000 20:00	MC	X	X	X	X	X	X	X
26	12-2-2000 22:00	16-2-2000 16:00	MC	X	X	X	X	X	X	X
27	29-11-2000 0:00	1-12-2000 10:00	MC				X	X	X	X
28	19-12-2000 6:00	21-12-2000 17:00	MC	X	X					
29	30-4-2001 9:00	2-5-2001 17:00	MC	X	X	X	X	X	X	X
30	9-12-2002 6:00	12-12-2002 6:00	MC		X	X	X	X	X	X
31	2-1-2003 16:00	4-1-2003 12:00	MC		X	X				
32	27-1-2003 10:00	30-1-2003 13:00	MC	X	X	X	X	X		X
33	3-2-2003 0:00	5-2-2003 16:00	MC				X	X	X	
34	17-2-2003 19:00	22-2-2003 23:00	MC						X	X
35	24-2-2003 1:00	28-2-2003 2:00	MC				X	X	X	X
36	1-12-2003 14:00	5-12-2003 20:00	ARST	X	X	X	X	X	X	X
37	14-12-2003 16:00	15-12-2003 10:00	MC	X	X	X	X	X		
38	15-12-2005 15:00	18-12-2005 9:00	MC		X	X	X			
39	18-12-2007 14:00	21-12-2007 8:00	MC			X	X	X	X	
40	2-1-2008 3:00	5-1-2008 19:00	MC		X	X	X	X	X	X
41	17-1-2010 16:00	22-1-2010 6:00	MC	X	X	X	X	X	X	X

*Local winter time (UTC+2), presented as day-month-year and hour.
[#]Simplified synoptic classification is based on Alpert et al. (2004) as described by Armon et al. (2020).

Table S2: WRF model settings and specifications.

	Outer nest	Middle nest	Inner nest
Domains			
Spatial resolution [km]	25 x 25	5 x 5	1 x 1
Temporal resolution [s]	~100	~20	4-8
Domain size [pixels]	100 x 100	221 x 221	551 x 551
Number of vertical layers	68	68	68
Model top [hPa]	25	25	25
Physics			
Cumulus scheme	Tiedtke (Tiedtke, 1989; Zhang et al., 2011)		-
Microphysical scheme	Thompson (Thompson et al., 2008)		
Radiative transfer scheme	RRTMG Shortwave and Longwave (Iacono et al., 2008)		
Planetary boundary layer scheme	Mellor–Yamada– Janjić (Janjić, 1994)		
Surface layer scheme	Eta Similarity Scheme (Janjić, 1994)		
Land surface model	Unified Noah Land Surface (Tewari et al., 2004)		
Input data			
Historic simulations	ERA-Interim reanalysis (Dee et al., 2011)		
"Future" (PGW) simulation	ERA-Interim + Δ climate from CMIP5 models		

Table S3: Coupled Model Intercomparison Project phase 5 (CMIP5) models used to compute the ensemble mean climate.

#	Model name	Latitude resolution [°]	Longitue resolution [°]	Number of vertical levels	Model top [hPa]
1	ACCESS1-0	1.25	1.88	17	10
2	ACCESS1-3	1.25	1.88	17	10
3	CCSM4	0.94	1.25	17	10
4	CESM1-BGC	0.94	1.25	17	10
5	CESM1-CAM5	0.94	1.25	17	10
6	CMCC-CESM	3.68	3.75	27	1
7	CNRM-CM5	1.39	1.41	17	10
8	CanESM2	2.77	2.81	22	1
9	GFDL-CM3	2.00	2.50	23	1
10	GFDL-ESM2G	1.52	2.50	17	10
11	GFDL-ESM2M	1.52	2.50	17	10
12	GISS-E2-H	2.00	2.50	17	10
13	GISS-E2-R	2.00	2.50	17	10
14	HadGEM2-AO	1.25	1.88	17	10
15	HadGEM2-ES	1.25	1.88	17	10
16	IPSL-CM5A-LR	1.89	3.75	17	10
17	IPSL-CM5A-MR	1.27	2.50	17	10
18	IPSL-CM5B-LR	1.89	3.75	17	10
19	MIROC-ESM	2.77	2.81	29	1
20	MIROC-ESM-CHEM	2.77	2.81	29	1
21	MIROC5	1.39	1.41	17	10
22	MPI-ESM-LR	1.85	1.88	22	1
23	MPI-ESM-MR	1.85	1.88	22	1
24	MRI-CGCM3	1.11	1.13	22	1
25	MRI-ESM1	1.11	1.13	22	1
26	NorESM1-M	1.89	2.50	17	10
27	NorESM1-ME	1.89	2.50	17	10
28	bcc-csm1-1	2.77	2.81	17	10
29	inmcm4	1.50	2.00	17	10

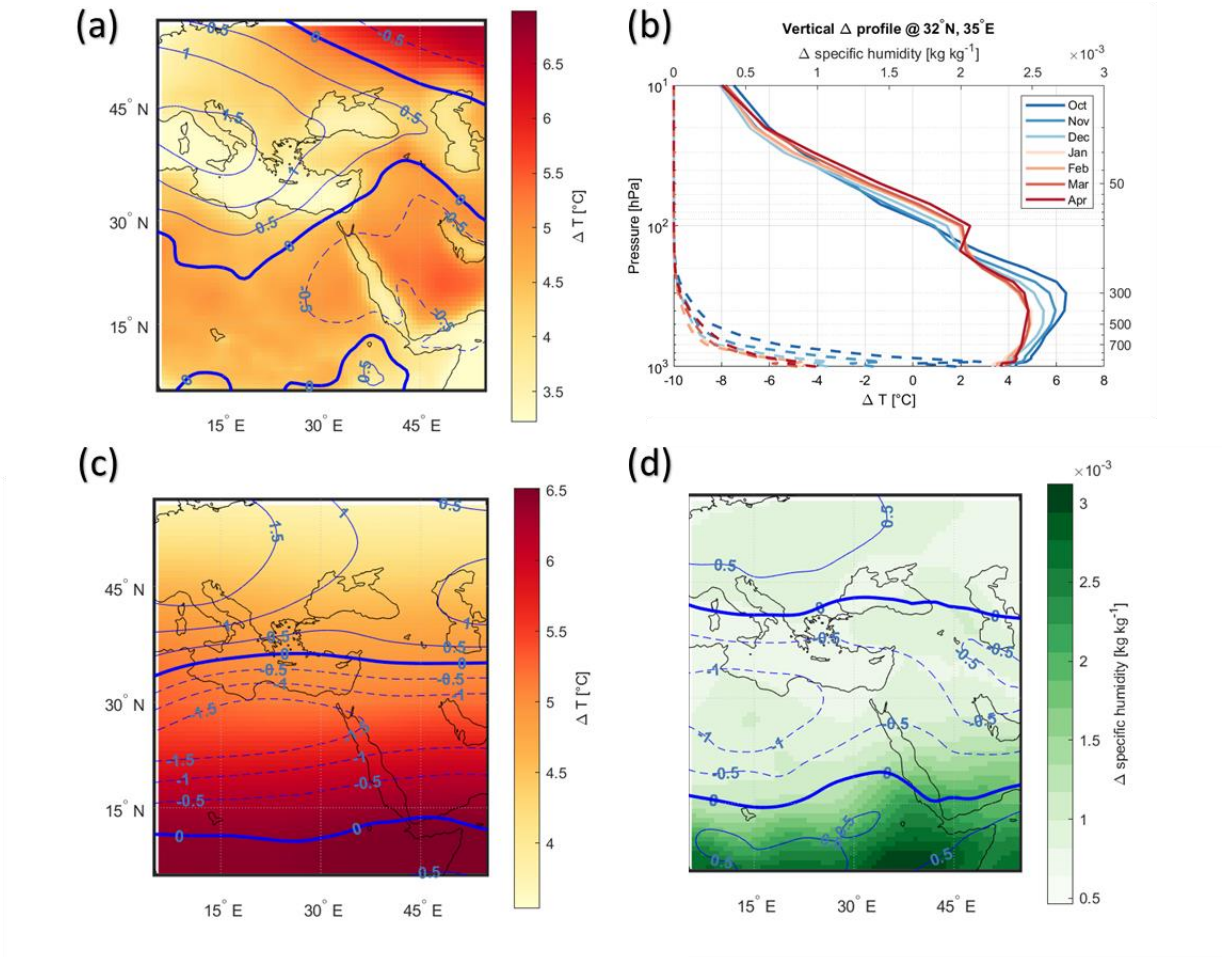

Figure S1. Examples of changes applied in "Future" (PGW) simulations based on ensemble mean of 29 CMIP5 models (Table S3). (a) Average change during the months with HPEs analyzed in this study (Oct through Apr; Table S1) in surface temperature (colors) and in sea-level pressure (contours). Dashed contours in panels a, c and d are negative signals. (b) Monthly vertical profiles of the change in temperature (solid lines, bottom horizontal axis) and in specific humidity (dashed lines, top horizontal axis) at the center of the study region (32°N, 35°E). Vertical changes were applied in each of the pixels along the study domain. (c) Average change (Oct through Apr) in upper-troposphere temperature (300 hPa; colors) and in the zonal (west-east) wind (contours). (d) Average change (Oct through Apr) in lower-troposphere specific humidity (850 hPa; colors) and in the zonal (west-east) wind (contours).

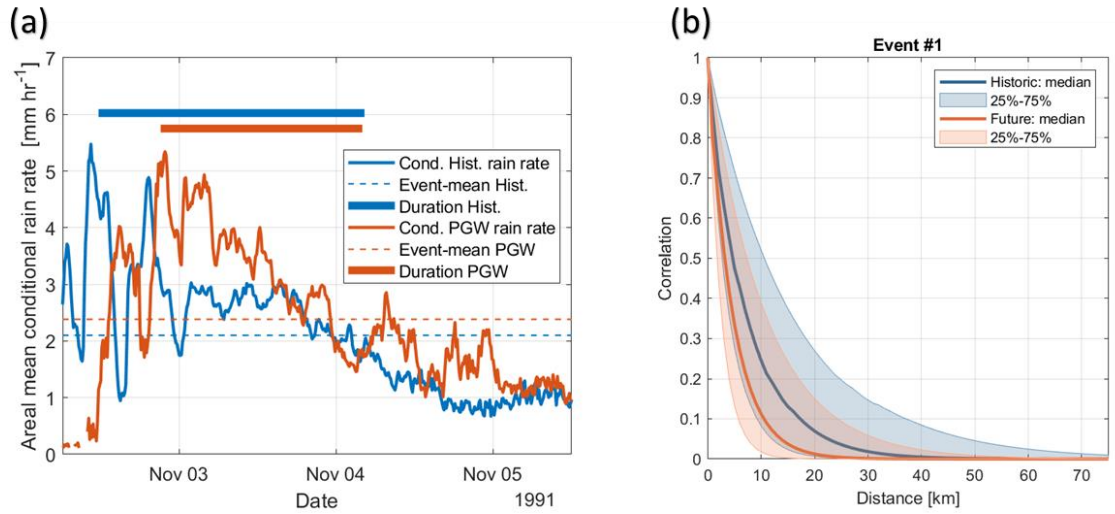

Figure S2. Additional rain properties of HPE #1. (a) Areal mean of 10-min conditional rain rates throughout the event. Dashed lines are the event-average values, and the bold, thick lines represent the duration of the event (the interval in which the central 90% of rainfall precipitated). (b) Autocorrelation structure of the 10-min convective rain fields for the first heavy precipitation event (HPE) in our collection, 2-5 Nov 1991. Curves are median values across 429 convective rain fields in the historic simulation (blue) and 407 in future simulation. Shaded areas represents the 25%-75% quantiles from each simulation.

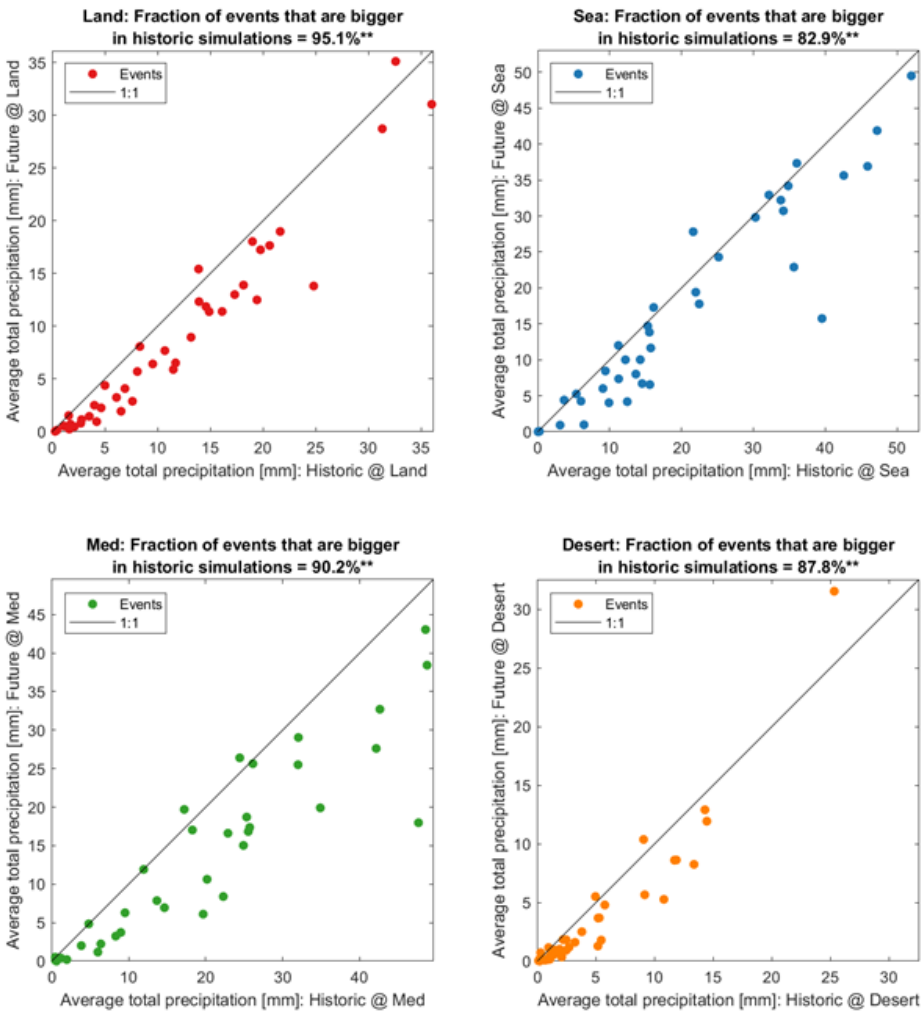

Figure S3. Comparison of future and historic rainfall accumulation of each of the 41 HPEs analyzed (as in Fig. 4a), computed separately for each of the sub-regions (Fig. 1b). Statistical significance, marked with ** in the panel titles, is based on paired (historic – future) tests (Sect. 2.4).

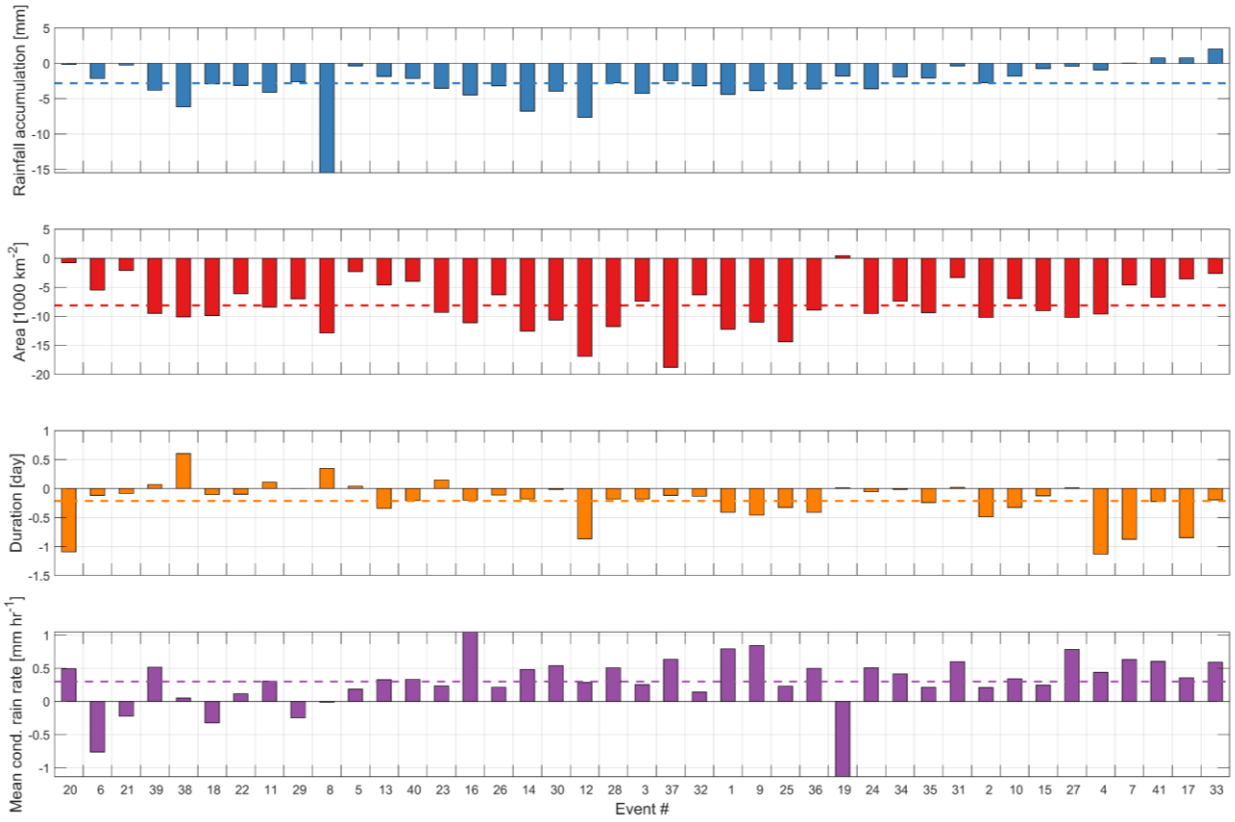

Figure S4. Change between future and historic simulations in event-average rainfall accumulation (blue), rainy area (red), event duration (orange), and mean conditional rain rate (purple), across the 41 HPEs analyzed. Events are ordered by their normalized changes in rainfall accumulation (see Fig. 5).

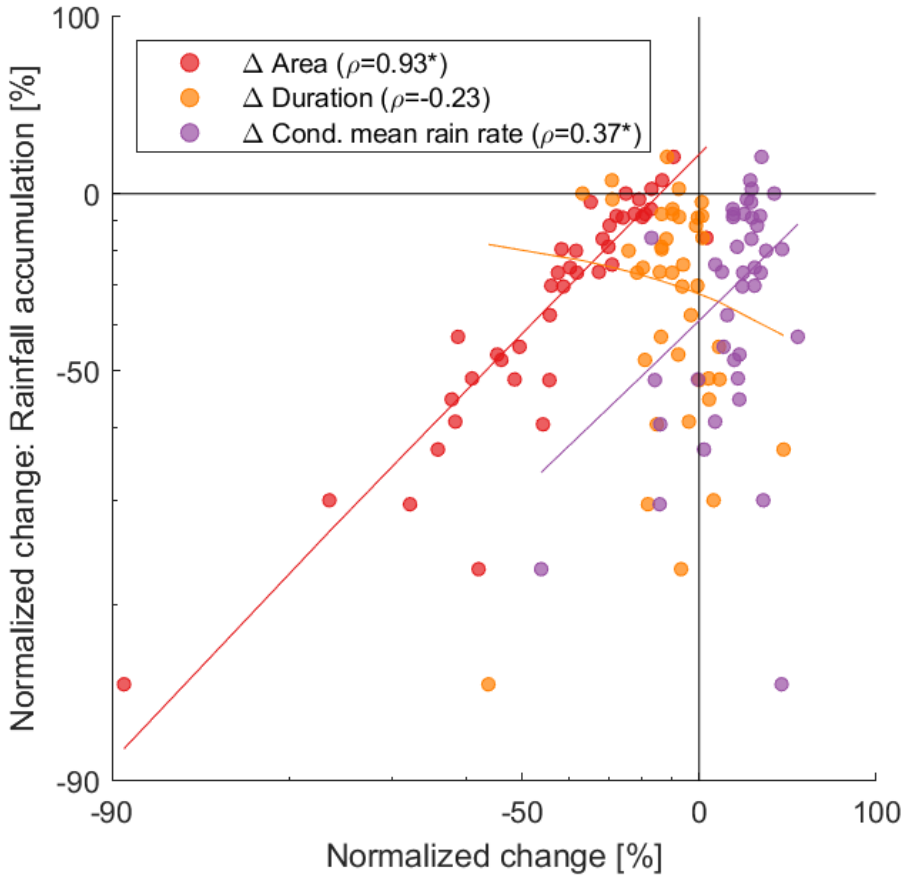

Figure S5. Association between the change in rainfall accumulation throughout the analyzed HPEs (vertical axis) and the different parameters shown in Fig. 5. Lines are the linear regressions between the parameters. Spearman's rank correlations are noted in the legend. Asterisks denote significant correlation.

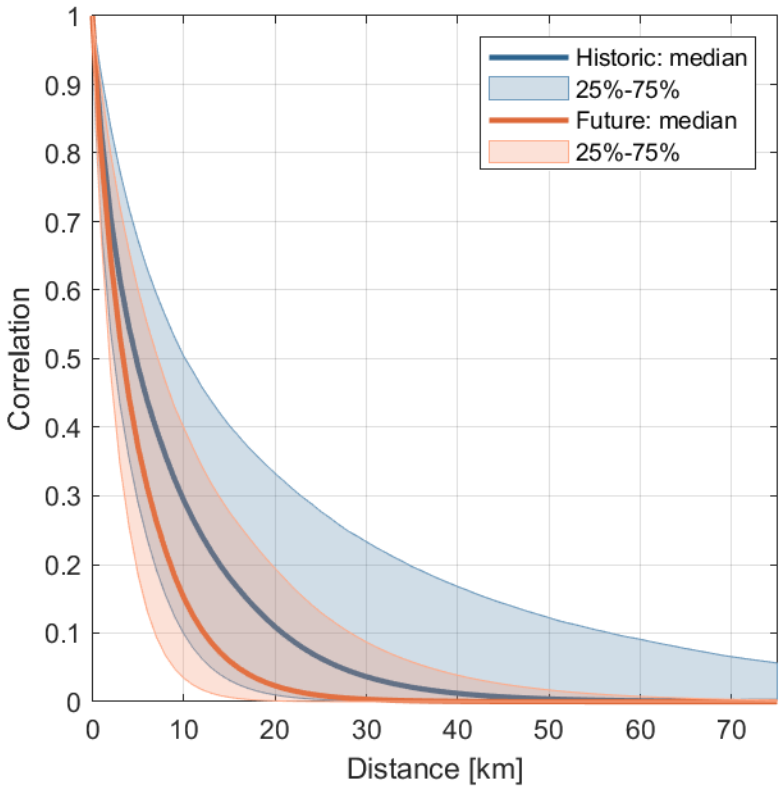

Figure S6. Spatial autocorrelation of the convective 10-min time steps for historic (blue) and future (orange) simulations. The number of convective time steps in historic and future simulations per event are 388±196 ($\mu \pm \sigma$) and 378±211, respectively. Calculations based on Marra and Morin (2018).

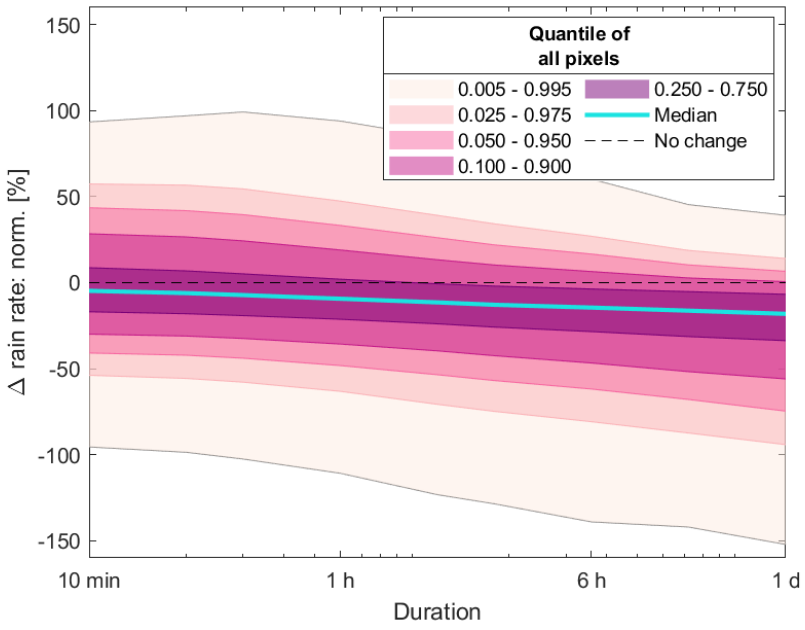

Figure S7. Quantiles among pixels (see Fig. 7) exhibiting different rain rate changes plotted versus the duration examined. Values are normalized to the areal mean value of each duration.

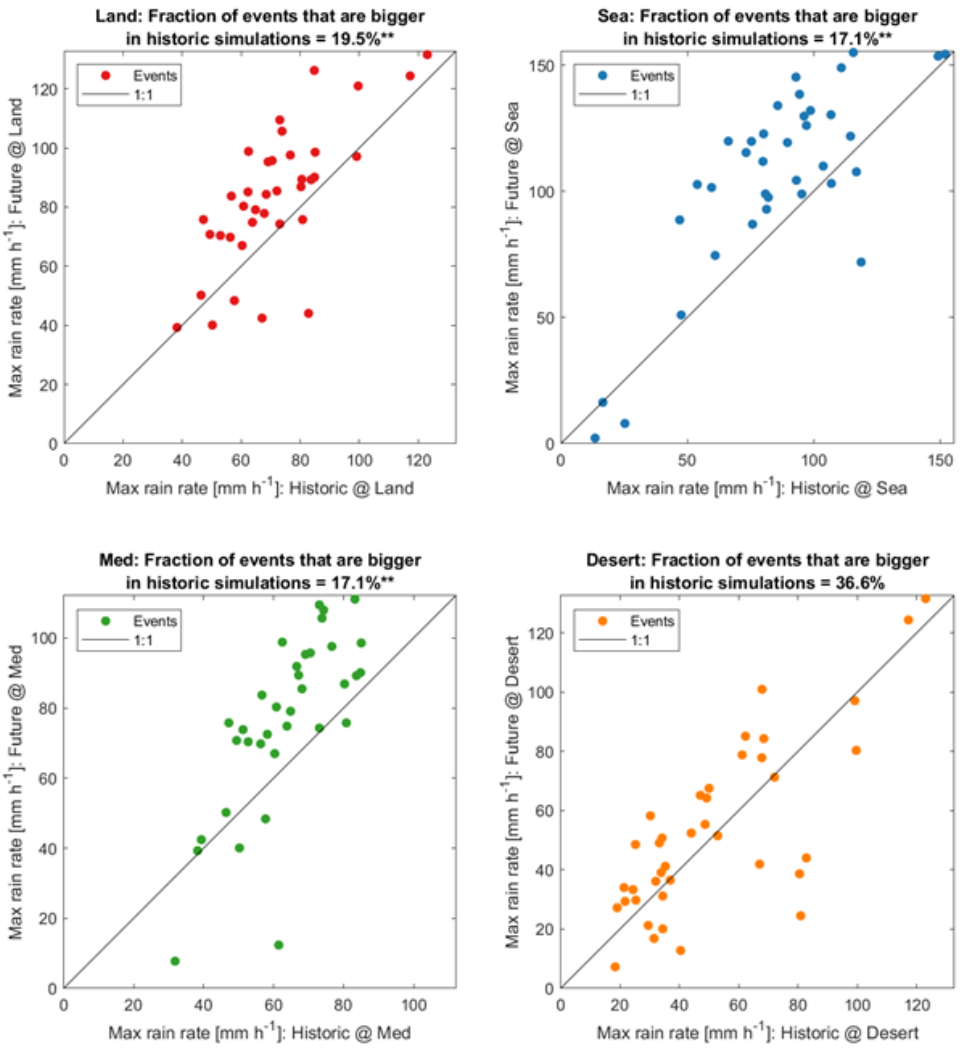

Figure S8. Same as in Fig. S3, but for maximal 10-min rain rate calculated throughout the pixels in each region and along all time steps. Maximum across all regions is in Fig. 4c.

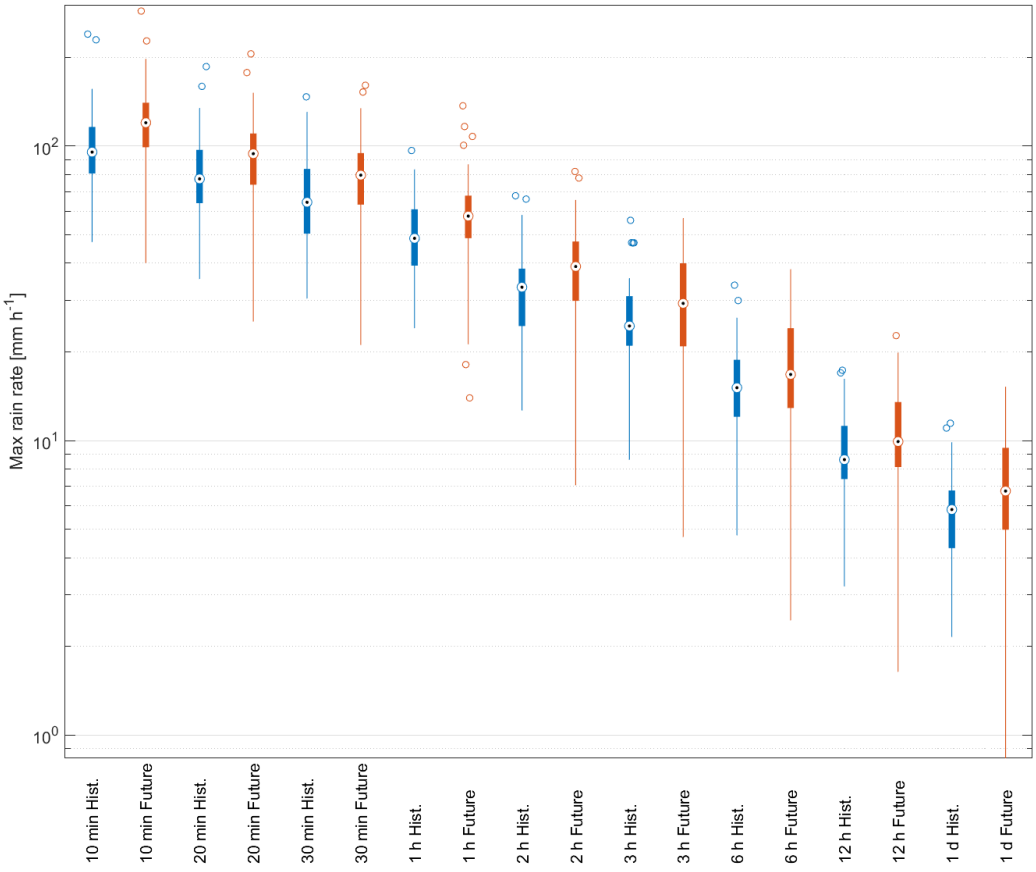

Figure S9. Boxplots of regionally maximal rain rates (across all pixels and time steps) for various durations. White circles with black dots are median values, boxes are the inter-quartile range (IQR), whiskers represents the full distribution except for cases where outliers (hollow circles) are found beyond the range of $\pm\, 1.5 \times IQR$ from the box.

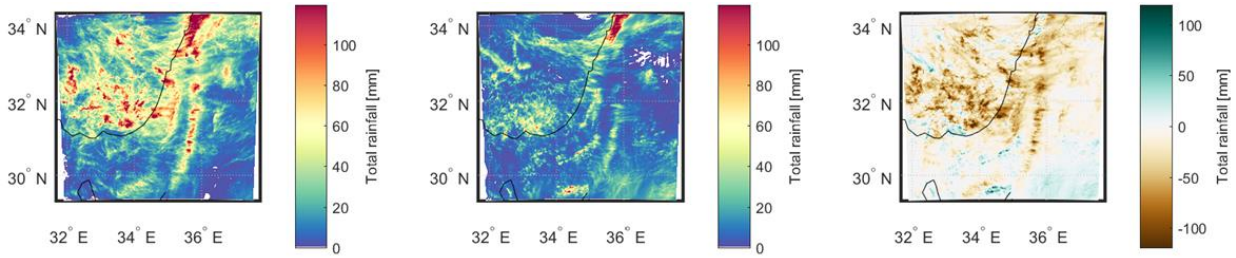

Figure S10. Rainfall in HPE#8 (1-7 Nov 1994). (a) Rainfall accumulation for the historic simulation (mean = 30.0 mm). (b) Total rainfall for the future (PGW) simulation (mean = 14.5 mm). (c) Difference between historic and future simulations (future – historic).

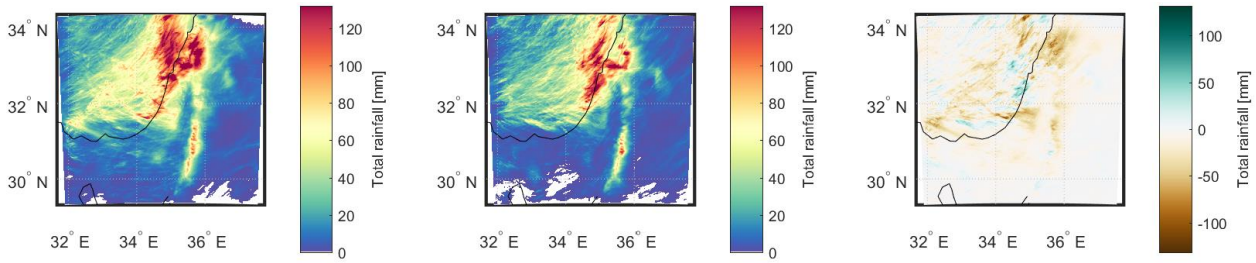

Figure S11. Same as figure S4, but for HPE#12 (4-9 Feb 1995). Historic simulation mean = 28.8 mm; future mean = 21.1 mm.

Movie S1. Animation of rain rate through time in historic (left) and future (right) simulations for HPE #1 (Table S1; Sect. 3.1).

Movie S2. Similar to Movie S1, but for HPE #8.

References from the Supporting Information

Alpert, P., Osetinsky, I., Ziv, B. and Shafir, H.: Semi-objective classification for daily synoptic systems: Application to the eastern Mediterranean climate change, Int. J. Climatol., 24(8), 1001–1011, doi:10.1002/joc.1036, 2004.

Armon, M., Marra, F., Enzel, Y., Rostkier-Edelstein, D. and Morin, E.: Radar-based characterisation of heavy precipitation in the eastern Mediterranean and its representation in a convection-permitting model, Hydrol. Earth Syst. Sci., 24(3), 1227–1249, doi:10.5194/hess-24-1227-2020, 2020.

Dee, D. P., Uppala, S. M., Simmons, A. J., Berrisford, P., Poli, P., Kobayashi, S., Andrae, U., Balmaseda, M. A., Balsamo, G., Bauer, P., Bechtold, P., Beljaars, A. C. M., van de Berg, L., Bidlot, J., Bormann, N., Delsol, C., Dragani, R., Fuentes, M., Geer, A. J., Haimberger, L., Healy, S. B., Hersbach, H., Hólm, E. V., Isaksen, L., Kållberg, P., Köhler, M., Matricardi, M., McNally, A. P., Monge-Sanz, B. M., Morcrette, J.-J., Park, B.-K., Peubey, C., de Rosnay, P., Tavolato, C., Thépaut, J.-N. and Vitart, F.: The ERA-Interim reanalysis: configuration and performance of the data assimilation system, Q. J. R. Meteorol. Soc., 137(656), 553–597, doi:10.1002/qj.828, 2011.

Giorgi, F. and Lionello, P.: Climate change projections for the Mediterranean region, Glob. Planet. Change, 63(2–3), 90–104, doi:10.1016/j.gloplacha.2007.09.005, 2008.

Iacono, M. J., Delamere, J. S., Mlawer, E. J., Shephard, M. W., Clough, S. A. and Collins, W. D.: Radiative forcing by long-lived greenhouse gases: Calculations with the AER radiative transfer models, J. Geophys. Res. Atmos., 113(D13), doi:10.1029/2008JD009944, 2008.

Janjić, Z. I.: The Step-Mountain Eta Coordinate Model: Further Developments of the Convection, Viscous Sublayer, and Turbulence Closure Schemes, Mon. Weather Rev., 122(5), 927–945, doi:10.1175/1520-0493(1994)122<0927:TSMECM>2.0.CO;2, 1994.

Marra, F. and Morin, E.: Autocorrelation structure of convective rainfall in semiarid-arid climate derived from high-resolution X-Band radar estimates, Atmos. Res., 200(September 2017), 126–138, doi:10.1016/j.atmosres.2017.09.020, 2018.

Nerini, D., Besic, N., Sideris, I., Germann, U. and Foresti, L.: A non-stationary stochastic ensemble generator for radar rainfall fields based on the short-space Fourier transform, Hydrol. Earth Syst. Sci., 21(6), 2777–2797, doi:10.5194/hess-21-2777-2017, 2017.

Seager, R., Osborn, T. J., Kushnir, Y., Simpson, I. R., Nakamura, J. and Liu, H.: Climate variability and change of mediterranean-type climates, J. Clim., 32(10), 2887–2915, doi:10.1175/JCLI-D-18-0472.1, 2019.

Tewari, M., Chen, F., Wang, W., Dudhia, J., LeMone, M. A., Mitchell, K., Ek, M., Gayno, G., Wegiel, J. and Cuenca, R. H.: Implementation and verification of the unified NOAH land surface model in the WRF model (Formerly Paper Number 17.5), in 20th Conference on Weather Analysis and Forecasting/16th Conference on Numerical Weather Prediction, pp. 11–15., 2004.

Thompson, G., Field, P. R., Rasmussen, R. M. and Hall, W. D.: Explicit Forecasts of Winter Precipitation Using an Improved Bulk Microphysics Scheme. Part II: Implementation of a New Snow Parameterization, Mon. Weather Rev., 136(12), 5095–5115, doi:10.1175/2008MWR2387.1, 2008.

Tiedtke, M.: A Comprehensive Mass Flux Scheme for Cumulus Parameterization in Large-Scale Models, Mon. Weather Rev., 117(8), 1779–1800, doi:10.1175/1520-0493(1989)117<1779:ACMFSF>2.0.CO;2, 1989.

Tuel, A. and Eltahir, E. A. B.: Why Is the Mediterranean a Climate Change Hot Spot?, J. Clim., 33(14), 5829–5843, doi:10.1175/JCLI-D-19-0910.1, 2020.

Tuel, A., O'Gorman, P. A. and Eltahir, E. A. B.: Elements of the Dynamical Response to Climate Change over the Mediterranean, J. Clim., 34(3), 1135–1146, doi:10.1175/JCLI-D-20-0429.1, 2021.

Zhang, C., Wang, Y. and Hamilton, K.: Improved Representation of Boundary Layer Clouds over the Southeast Pacific in ARW-WRF Using a Modified Tiedtke Cumulus Parameterization Scheme, Mon. Weather Rev., 139(11), 3489–3513, doi:10.1175/MWR-D-10-05091.1, 2011.